

THS

LINARY Michigan State University

This is to certify that the

thesis entitled

Fast Fragment Emission in Nuclear Collisions

presented by

Silvana P. Angius

has been accepted towards fulfillment of the requirements for

M. S. degree in Physics

Major professor

Date 25 February 83

O-7639

MSU is an Affirmative Action/Equal Opportunity Institution



RETURNING MATERIALS:
Place in book drop to remove this checkout from your record. FINES will be charged if book is returned after the date stamped below.

FAST FRAGMENTS EMISSION IN NUCLEAR COLLISIONS

Ву

Silvana P. Angius

A THESIS

Submitted to
Michigan State University
in partial fulfillment of the requirements
for the degree of

MASTER OF SCIENCE

Department of Physics and Astronomy

1983

ABSTRACT

FAST FRAGMENT EMISSION IN NUCLEAR COLLISIONS

By

Silvana P. Angius

Inclusive spectra for various light fragments obtained from α -particle induced reactions, and for heavy fragments from 40 Ar induced reactions have been analyzed according to the single moving source model. The source is characterized by a temperature and a velocity, and is assumed to emit fragments isotropically in its rest frame.

This parametrization, already known to be successful for heavier projectiles, is proven valid also in the case of α -particles. A rather good agreement is obtained for heavy fragments, too, indicating that it is possible that fragments heavier than ⁴He are emitted in a similar process.

The present analysis helps to reinforce the validity of a localized, thermal source, whose existence is important to the development of thermal and hydrodynamical description of heavy-ion collisions. The emission of heavy clusters from a thermal source may be of interest in the study of phase transitions in nuclear matter.

ACKNOWLEDGMENTS

I wish to thank my advisor, professor David Scott, who gave me the opportunity to work on this project, and did so in many ways.

I should like to express my gratitude to Olaf Scholten, who helped me so much with many useful discussions, with advice and especially with his patience and friendship.

Finally, to Erich Ormand, who made most of the figures, spent hours (and nights) printing and adding 'alphas' to the text and had confidence when I did not, my most affectionate thank you.

TABLE OF CONTENTS

																				page
List o	f '	Tab	les.		•	•	•		•	•	•	•	•	•	•	•	•	•	•	iv
List o	f	Fig	ures		•	•	•		•	•	•	•	•	•	•	•	•	•	•	v
Chapte	r	1.	INTRO	DUC	TIC	N	•		•	•	•	•	•	•	•	•	•	•	•	1
Chapte	r :	2.	EMISS	ION	FF	ROM	A	TH	ERM	IAL	S	ου	RC	E	•	•	. •	•	•	8
			2.1.	Inv	ari	.an	t (Cro	88	Se	ct	io	n	P1	.ot	.s	•	•	•	8
			2.2.	Der	iva	ti	on	of	th	e	Di	st	ri	.bu	ıti	.or	١.	•	•	12
			2.3.	The	Nu	ıcl	ea	r F	ire	ba	11	M	Ođ	el	. •	•		•	•	18
Chapte	r :	3.	DATA	ANA	LYS	sis	Al	ND I	RES	UL	TS	•	•	•	•	•	•	•	•	29
Chapte	r	4.	CONCI	USI	ONS	3 .	•		•	•	•	•	•	•	•	•	•	•	•	44
Append	ix	Α.	RELA CROS									•				•	•	•	•	52
Append:	ix	в.														_		_		56

LIST OF TABLES

TABLE							P	A GE
2.1	Average number of nucleons in the fireball (N_{tot}) , average number of protons (Z_{tot}) , and Coulomb energies for the system analyzed	•	•	•	•	•	•	27
3.1	Summary of the relevant parameters for all the systems analyzed	•	•	•	•	•	•	37

LIST OF FIGURES

Figure		Page
2.1	Rapidity plot for the α+Ta→p reaction. The solid lines are calculated for a source of temperature T=26.9 MeV moving with velocity v/c =0.184. The dotted lines are meant to guide the eye through the experimental points	. 9
2.2	Rapidity plot for the a+Ni → p reaction. The solid lines are calculated for a source of temperature T=7.74 MeV and velocity v/c =0.086. The dotted lines are drawn trough the experimental points to guide the eye	. 10
2.3.	Proton spectra fitted with the surface Maxwellian distribution. The resulting parameters are indicated	. 14
2.4.	Deuteron spectra fitted with the surface Maxwellian distribution. The resulting parameters are indicated	. 15
2.5	Formation of a fireball. The over- lapping nucleons from target and projec- tile are swept out to form a thermal source moving with velocity	. 20
2.6	Geometrical quantities calculated for the system $\alpha+Ni$, as a function of impact parameter. (a) number of protons in the fireball, (b) total number of nucleons, (c) weight given to each impact parameter	. 24
	Geometrical quantities calculated for the system Ar+U, as a function of impact parameter. (a) number of protons in the fireball, (b) total number of nucleons, (c) weight given to each impact parameter.	. 25

Figure		Page
2.8	Geometrical quantities calculated for the system $\alpha+Ta$, as a function of impact parameter. (a) number of protons in the fireball, (b) total number of nucleons, (c) weight given to each impact parameter	. 26
3.1	Proton spectra for the a+Ta reaction, at an incident energy of 720 MeV. (a) single moving source fit; the points at 30 and those below 30 MeV were not included in the fit. (b) Three-source fit, including all angles and energies. The final parameters obtained for the intermediate rapidity source are indicated	. 32
3.2	Deuteron spectra from the $\alpha+Ta$ reaction at 720 MeV. The final parameters, from which the solid curves are obtained, are T=26.86 MeV, $v/c=0.169$, $\sigma_0=0.932$ b	. 33
3.3	³ He spectra obtained from the reaction α +Ta at 720 MeV. The best fit gave: T=26.83 MeV, v/c =0.166, σ_0 =0.119 b	. 34
3.4	The experimental proton spectra obtained from the reaction $\alpha+\mathrm{Ni}$ at 25 MeV per nucleon are plotted with the curves obtained from the χ^2 -fit (solid lines) with the following parameters: T=7.74 MeV, $v/c=0.086$, $\sigma_0=1.206$ b. The points at 25 were not included in the fit.	. 35
3.5	Experimental and calculated curves for the ^{11}B fragments obtained from the reaction Ar+U at 100 MeV per nucleon. The 'best fit' parameters are: T=26.6 MeV, $v/c=0.100$, $\sigma_0=0.369$ b. The points at 35 were not included in the fit	. 36
3.6	Source temperatures obtained from a χ^2 -fit. The solid points are for the systems analyzed in this work, the others are taken from reference 19	. 39
3.7	Source velocities obtained from a χ^2 -fit. The solid points are for the systems discussed in the present work; the others are taken from reference 19	. 4 Ø
3.8	Normalized multiplicaties for emission of protons in a-particle induced reactions, as a function of the incident energy per nucleon	42

Figure		Page
4.1	(a) angular dependence of the temperatures obtained for the $Ni(\alpha,\alpha'p)$ reaction. (b) possible mechanism causing the asymmetry observed in (a)	46
4.2	Weighted cross sections as a function of the fragments mass. The points for A ≤ 4 are taken from the reaction Ne+Au at 100 MeV/nucleon, normalized for comparison with B and C, obtained from Ar+U at the same incident energy. The curve	
	represents the prediction of the coalesence model, with $p_0 = 130 \text{MeV/c}$	48
4.3	The energy-density plane for nuclear matter. The curves are isentropes	51
B.1	Definition, in the (δ, ν) plane, of the regions where the four F functions must be applied	58

Chapter 1

INTRODUCTION

At low incident energies, the emission of light particles in heavy ion induced reactions has been shown to occur mainly from the compound nucleus 1,2), but for increasing beam velocities, the experimental cross sections extend up to rather high energies with significant yields, the decrease being some orders of magnitude less than would be expected for emission from the compound nucleus. These light fragment energy spectra have been variously interpreted in terms of pre-equilibrium emission 3,4), intranuclear cascade models 5,6), PEPS (prompt emission of light particles) 7,8), hot spot formation 9-13) or nuclear fireball or firestreak models 14-17). They are therefore of great interest as potential sources of information on localized depositions of energy in a nucleus.

The justification for the thermal model approach comes from the fact that the high energy tails of the spectra observed for light particles $(p,d,t,\alpha)^{18-21}$ and, more recently, for heavier fragments 22 , display an exponential slope characteristic of thermal emission, if a temperature higher than the classical compound nucleus temperature $(T=\sqrt{8E^*/A})$ is assumed. Clearly, a much higher temperature can be attained if only a limited number of the nucleons in the target and in the projectile are involved, i.e., if an entity like a hot- spot or a fireball is formed. Also, in

central collisions, a rather large number of nucleons interact, and it seems that some degree of thermalization occurs after only a few interactions.

All thermal models assume the existence of one or more sources, isotropically emitting particles in their rest frames. The simplest thermodynamic model assumes the presence of only one source at temperature T and moving with velocity parallel to the beam direction, irrespective of how it is produced. The temperature is readily deduced from the slope of the energy spectra (e.g. from the spectrum at 90° , where the effects due to the velocity are negligible) and the velocity can be obtained from the fit of the spectra at different angles.

More detailed models attempt to explain the formation, the nature and the decay of the source. In the hot-spot is identified with a "hot" region model, the source created in the zone of impact between projectile and target. In this approach, the heat localized in the hot spot spreads into the adjacent nuclear matter according to a diffusiontype process and the local temperature is measurable by spectra of the particles emitted during observing the this pre-equilibrium phase. In this description 23,24), link is established between pre-equilibrium phenomena and the transport properties of nuclear matter, by introducing the idea of heat conductivity (K) in nuclear matter. The classical diffusion equation for the temperature T has the form

$$\rho c_{p} \frac{\partial T}{\partial t} = \text{div (K grad T)}$$
 (1.1)

where ρ is the density of nuclear matter, and c_{p} the specific heat at constant pressure; this equation can be to describe the evolution towards equilibrium. According to Tomonaga²⁵⁾, the nucleus is assumed to be a four-component Fermi gas and the transport coefficients are obtained from the linearized Boltzmann equation; the thermal conductivity is then proportional to the mean free path for nucleon-nucleon scattering, \bigwedge : $K \propto c_{D}^{N} N_{F} \bigwedge$. This implies that \wedge must be small in order to create a hot spot. At low temperatures, \(\) will be large, so K will be large too and the diffusion of heat too fast for the effect of the hot spot to be appreciable. Incidentally, the requirement of a short mean free path makes a microscopic description like the TDHF theory impossible to apply to this case, since the validity of such an approach is based on the assumption of a long mean free path. It has been suggested 26) that the TDHF approach may still be valid up to energies per particle of the order of $E_{\mathbf{p}}$, the Fermi kinetic energy per particle (2 37 MeV). Even so, for decreasing \wedge the TDHF approximation is no longer applicable.

The fireball model can be seen as a natural extension of the idea of hot spot at higher energies, if the excited zone emerges as a separate entity. The geometry, kinematics and thermodynamics of the fireball allow the calculation of

the number of participant nucleons and of the velocity and decay of the source.

Such macroscopic thermal models can successfully fit the experimental cross sections over a large range of incident energies, but they fail to explain some of the features observed in the data, especially in the low energy portions of the spectra and the data at the most forward angles. In these cases, it is possible that other mechanisms of emission are taking place. It has also been suggested that the high energy light particles can be produced from one or two collisions before thermalization takes place.

Additional information can be obtained from the study of the emission of composite fragments, which cannot be produced in single collisions. The slopes observed for energy spectra of different fragments, for a given reaction, are similar. In the context of a thermal model, this implies that the fragments are all emitted from a source of well defined temperature. Moreover, it is easy to relate the composite particle spectra to the corresponding spectra for protons. If E is the total energy of a cluster of mass A, the cross sections will be proportional to exp $\left(-\frac{E/A}{T}\right)^A$, which is the single nucleon (proton) cross section raised to It is interesting to note that the same the A-th power. power law for composite fragment cross sections is derived the coalescence model 15,27-30, where the probability of formation of such a particle is related to the probability or more nucleons within a sphere of of finding two

radius p_{O} (the coalescence radius), centered at p, in momentum space. This power law has been verified for light particles (d, t, 3 He) over a large range of incident energies 28), but the α -particle cross sections have been found to follow a different trend compared to deuteron and triton spectra 19). In particular, it appears that the α /p ratio decreases steadily with increasing incident energy, and has values larger than 1 at low energies, while the d/p and t/p ratios remain approximately constant over the whole range. Such a result seems hard to explain within the coalescence model, but it is predictable in a thermal (gas) model, considering the large binding energy of 4 He.

It has also been suggested 31) that this behaviour could be attributed to the onset of a liquid-gas phase transition which may develop at a temperature around 20 MeV. To further test this assumption, it would be useful to study the emission of heavier clusters (A>4), whose formation should be strongly disfavoured in the simple (non-interacting) gas model. A hydrodynamic description, including compression and expansion, could predict such phase transitions, possibly also at higher densities, where more exotic states of nuclear matter could be obtained.

The purpose of this thesis was to test the applicability of a simple thermal model (single, fireball-like source, emitting isotropically in its rest frame) to data obtained for light fragments emitted in α -particle induced reactions and to heavy cluster spectra. The interest in

applying the framework developed for heavy ions to a-particles rests in the fact that a thermal source generated by a light projectile would be composed of a limited number of nucleons and the possibility that some degree of thermalization be reached in such a small system would be encouraging evidence for the validity of the basic assumptions the thermodynamic approach. Also, the results made in obtained for α -particles should be comparable to those for heavier projectiles, if the properties of the source, its formation and decay depend only on the incident energy per nucleon, and the process is such that all memory of the initial system is lost, as it should be in the creation of a thermal source. Also, studies with a-particles can be conducted over a wider range of energies than is generally available with heavier beams. In the application to heavy fragments (A>4), it is particularly interesting to compare the total cross sections obtained with the predictions, e.g., of the coalescence model and with the possibility of condensation which may occur in a liquid-gas phase transition. In the case of heavy clusters, the previous remarks about thermal emission are also valid. The question in this case is whether the temperatures and velocities obtained for fragments of different mass follow the same trend. If this is the case, the hypothesis that different are emitted from a source of well defined temfragments perature, and therefore the assumption that such a source may indeed exist, gains additional support.

The next chapter will deal with the justification and the derivation of the formulae used, an exposition of the theoretical ideas behind the moving source model (fireball model), and the description of some assumptions made in the calculations. The results obtained for the systems analyzed in this work (i.e. tem perature and velocity of the sources and total cross sections) will be described in Chapter 3, together with a comparison with the analogous results obtained for different systems and energies. An interpretation of the results, their meaning and possible consequences will be given in Chapter 4.

Chapter 2

EMISSION FROM A THERMAL SOURCE AND FIREBALL MODEL

2.1. Invariant Cross Section Plots

In general, the fragments produced in a collision between high energy heavy ions originate from several different sub systems in which the total system of projectile plus target separates. For example, emission can originate from the nuclear fireball formed by the overlapping sections of target and projectile, from the remaining part of the target (spectator) and/or fragmentation of the projectile, or from the explosion of the whole system.

Particles emitted from different mechanisms present different distributions in energy and momentum. In particular, if we analyze the distribution of the relativistically invariant cross sections in the p, p plane (where p and p are the components of the momentum perpendicular and parallel to the beam direction, respectively), the contributions from different sources should appear. In the case of relativistic particles, the perpendicular momenta should be plotted vs. the rapidity along the beam direction, defined as

$$Y_{\parallel} = \tanh^{-1} \beta_{\parallel} = \frac{1}{2} \ln \left[(E+p_{\parallel})/(E-p_{\parallel}) \right]$$
 (2.1)

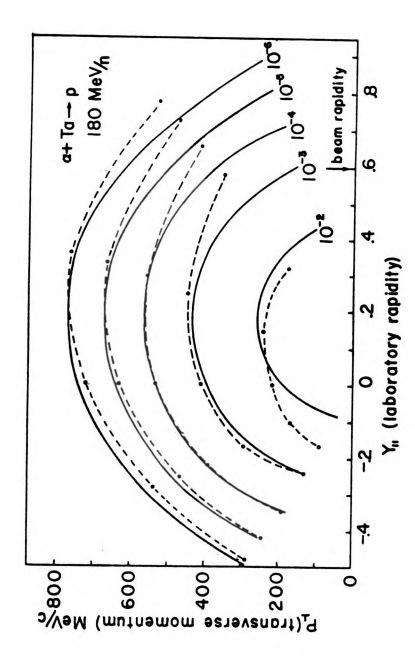
The contour lines of constant invariant cross section in the \mathbf{p}_{\parallel} , \mathbf{Y}_{\parallel} plane are invariant with respect to Lorentz

transformations, except for a shift along the rapidity axis. In this way, an isotropic emission in the source frame will appear isotropic when the experimental cross section (obtained in the laboratory frame) are plotted, and the transformation will simply result in a translation of the curves along the Y_{\parallel} axis, by an amount equal to the rapidity of the source. In Figures 2.1 and 2.2 the rapidity plots are shown for the systems $\alpha+Ta+p$ at 180 MeV/nucleon and $\alpha+Ni+p$ at 25 MeV/nucleon. Here, the invariant cross sections

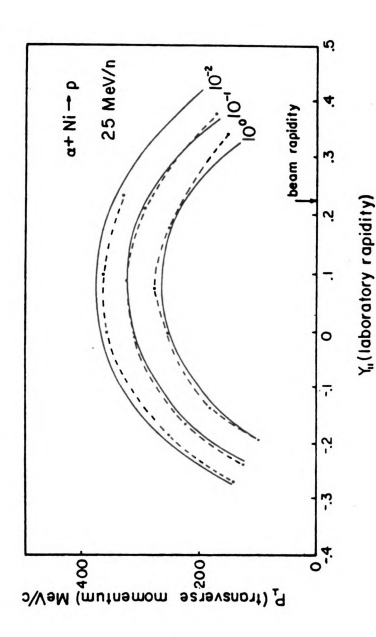
$$E \frac{d^3}{dp^3} = \frac{1}{p} d^2 \frac{\sigma}{dE d\Omega}$$

are plotted in the $Y_{||}$, $p_{||}$ plane. From the shapes of the curves, the relative spacing between curves corresponding to a constant factor in cross section, and the position on the $Y_{||}$ -axis around which the curves are centered, it is possible to estimate qualitatively whether the single source model with a distribution proportional to $\exp(-E/T)$ is reasonable, and in which range of angles and energies.

The rapidity plot for the α +Ta reaction is shown in Figure 2.1; it displays contours of equal cross section centered at a rapidity of about 0.2, corresponding to the rapidity of the main source. The asymmetry at the lower angle (30°) suggests the presence of a second source of higher rapidity, emitting in the forward direction. The displacement of the contour at 10^{-2} sr/MeV with respect to the



Rapidity plot for the a+Ta+p reaction. The solid lines are calculated for a source of temperature dotted lines are meant to guide the eye through T=26.9 MeV moving with velocity \$=0.184. The the experimental points. Figure 2.1.



temperature T=7.74 MeV and velocity \$=0.086. solid lines are calculated for a source of Rapidity plot for the a+Ni + p reaction. trough experimental points to guide the eye. The dotted Figure 2.2.

others must also be noticed; it indicates that the low energy portions of the spectra may be due to a different process, since the curve is centered around a much lower rapidity. The beam rapidity has also been indicated in the figure at approximately 0.6.

This qualitative analysis suggests that the single moving source approximation is justified in this case, for angles $\geq 60^{\circ}$ and for energies above 30 MeV.

An analogous plot for the reaction $\alpha+\mathrm{Ni} \to \mathrm{p}$ at 25 MeV per nucleon (see Figure 2.2) shows the correct spacing of the contours of constant cross section. The curves, in this case, are centered at a rapidity of approximately 0.08, whereas the beam rapidity, indicated by an arrow in the figure, is 0.23.

2.2 <u>Derivation of the Distribution</u>

The idea of approximating the experimental distributions with the distribution from a single moving source is justified within the range of angles and energies indicated by the rapidity plots. The data at very forward angles ($\geq 60^{\circ}$) and at low energies (<30 MeV) must be excluded from the fit, since they contain important contributions from mechanisms different from the one investigated in this work.

The next step is the assumption of a particular distribution of energies (or momenta) in the rest frame of the source, and the transformation of this distribution to the laboratory frame where the source is moving with velocity v.

The energy distribution in the source is assumed to be of the thermal form, characterized by the Boltzmann function exp(-E/T), where E is the total energy of a particle and T the temperature of the source (in energy units). factor in front of the exponential can be proportional $\sqrt{\text{E}}$ or to E. The first case is usually adopted for 'volume' emission, i.e. when the fragments are assumed to be emitted from the entire volume of the source, as in the case of a fireball, which is supposed to break up into many fragments, or in the case of projectile fragmentation. The distribution with a linear E factor (or 'surface Maxwellian') corresponds to a nonrelativistic Maxwell-Boltzmann distribution for particles emitted from the face of a hot object. The extra factor depends on the fact that faster particles are more likely to be emitted in any interval. It has been observed that the pregiven time exponential factor contains important information about the details of the process leading to a thermal spectrum.

For the analysis of the data presented in this work, the 'volume' form (\sqrt{E}) has been chosen, since the energies involved are high enough to lead to volume emission (larger than 20 MeV per nucleon, as suggested by Goldhaber in reference 32). Also, this distribution is consistent with previous analyses, results of which are compared with those of the present work. For some set of data both distributions have been used, and the resulting curves and values indicate that a better agreement is obtained with

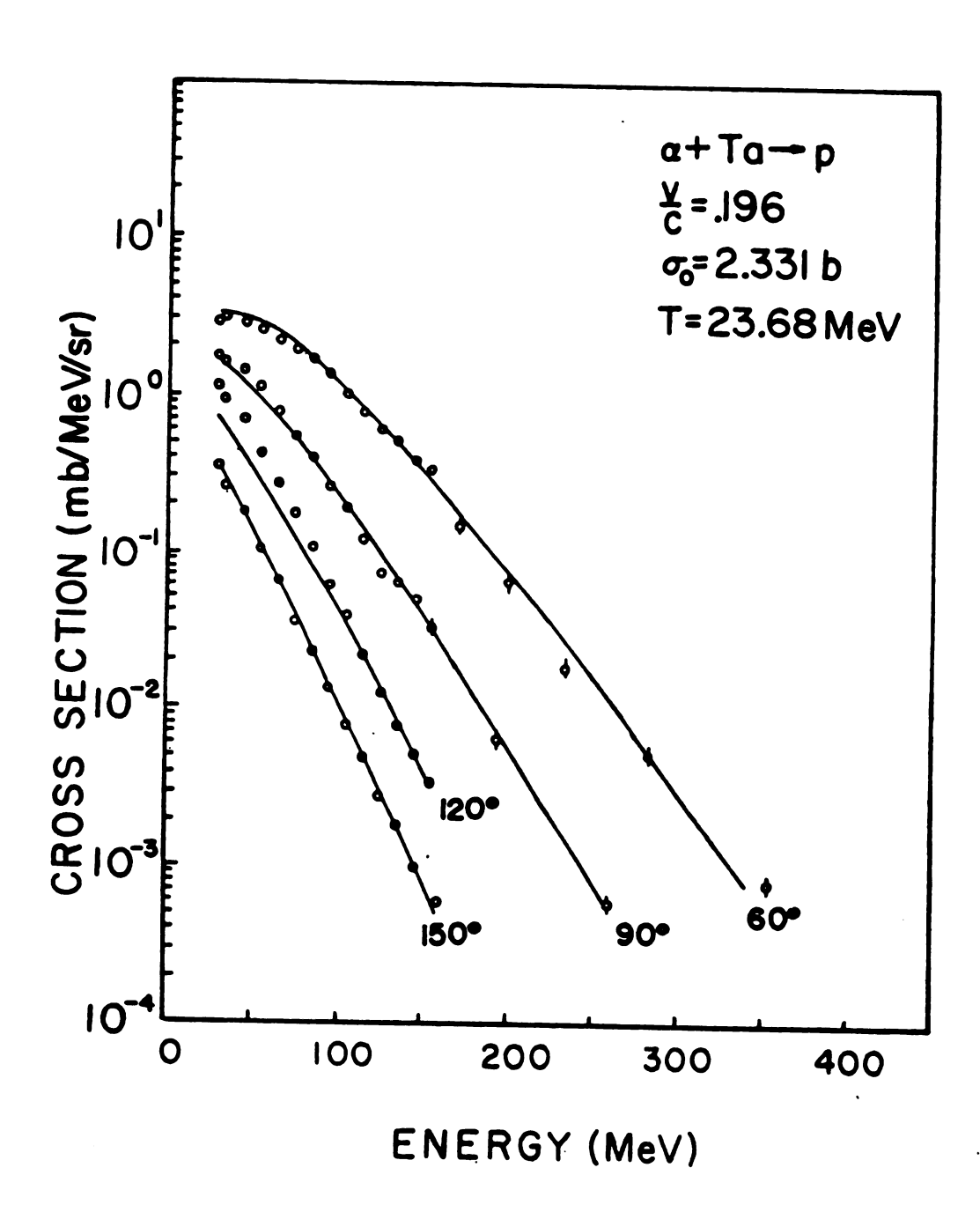


Figure 2.3. Proton spectra fitted with the surface Maxwellian distribution. The resulting parameters are indicated.

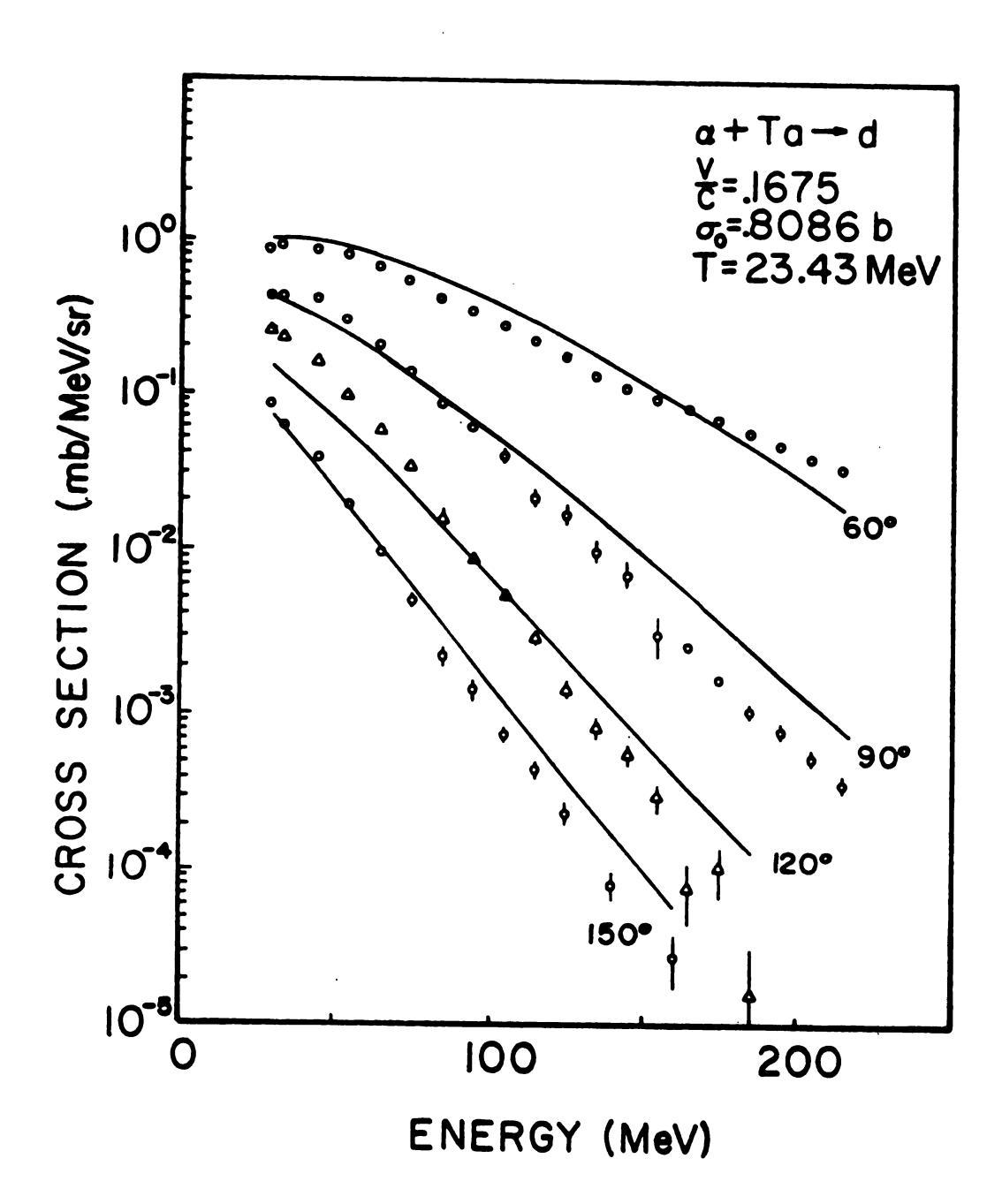


Figure 2.4. Deuteron spectra fitted with the surface Maxwellian distribution. The resulting parameters are indicated.

the surface factor. Since there is no striking improvement in most cases, expecially for fragments heavier than protons, and since it is doubtful which kind of emission is actually taking place, the factor \sqrt{E} has been used thoughout the analysis. In Figures 2.2 and 2.3 the proton and deuteron spectra from $\alpha+Ta$, fitted with the surface Maxwellian distribution, are shown for comparison with Figures 3.1 and 3.2. It is also worth mentioning that the parameters obtained with the 'surface' form, even though systematically different (e.g. the temperatures are always lower), do not differ by more than about 15% from the parameters obtained with the

Therefore, the energy distribution in the source has the following form:

$$\frac{d^2\sigma'}{dE'd\Omega'} = \frac{\sigma_0}{2(\pi T)^{3/2}} \sqrt{E'} e^{-E'/T}$$
 (2.2)

where the factor $\alpha/2(\pi T)^{3/2}$ has been evaluated so that the term σ_0 represents the total cross section:

$$\sigma_0 = \int_0^{\infty} dE \int_{\Omega} \frac{d^2 \sigma}{dE \ d\Omega} \ d\Omega$$

Also, a correction for the Coulomb energy due to the repulsion from the charged source must be introduced. The Coulomb force has been assumed to act radially, so that its effect is essentially to cut off that part of the spectrum where the kinetic energy of the particle is less than or equal to

the Coulomb energy $(K \geq E_C)$. This reflects the physical fact that the energy of a particle after the emission (at the infinite distance of the detector from the source) cannot be less than the Coulomb energy and cannot be equal to E_C , since this would correspond to a particle with zero kinetic energy in the source, and such a particle would not be emitted at all. Therefore, the distribution becomes:

$$\frac{d^2\sigma'}{dE'd\Omega'} = N\sqrt{E'-E_C} \Theta(K'-E_C) e^{-\frac{E'-E_C}{T}}$$
(2.3)

where E'=K'+m is the total energy of the fragment of mass m in the source frame, at infinite distance from the source, and the @ -function gives the required cut-off.

This distribution must be transformed to the laboratory frame to be compared with the experimental spectra. A derivation of the transformation is given in Appendix A. The result is:

$$\frac{d^2\sigma}{dE\ d\Omega} = \frac{p}{p'} \frac{d^2\sigma'}{dE'\ d\Omega'} \tag{2.4}$$

where the primed coordinates refer to the source frame and the unprimed ones refer to the laboratory frame.

Now we must express p, p', K', and E in terms of known quantities in order to obtain the distribution which will be used to fit the data. The first useful relation is

$$E' = y(E - \frac{v}{C} p \cos \theta)$$
 (2.5)

which gives the relation between the total energy of a fragment in the source frame and quantities measured in the laboratory frame, viz. K and θ . Here v/c is the velocity of the moving source. Also, we have:

$$p' = \sqrt{E'^2 - m^2} = \sqrt{y^2 (E - \frac{v}{c} p \cos\theta)^2 - m^2}$$
 (2.6)

and E= K+m. The final expression for the distribution in the laboratory frame in terms of K and Θ becomes:

$$\frac{d^{2}\sigma}{dE \ dQ} = \frac{\sigma}{2(\pi T)^{3/2}} \sqrt{\frac{[(K+m)^{2}-m^{2}][Y(K+m-\frac{v}{c} \ p \ cos\theta) \ -E_{c}]}{Y^{2} \ (K+m-\frac{v}{c} \ p \ cos\theta)^{2} \ -m^{2}}}$$

$$\exp\left[-\frac{y(K+m-\frac{v}{C} p \cos \theta) - E_{C}}{T}\right]$$
 (2.7)

where $y(K+m-\frac{v}{C} p \cos\theta)-m\geq E_{C}$.

2.3. The Nuclear Fireball Model

In the analysis of the data and in the interpretation of the results, some assumption have to be made about the number of nucleons in the source in order to estimate the Coulomb energy which appears in the distribution, and also to have a criterion of normalization which allows the results obtained for differerent systems to be compared.

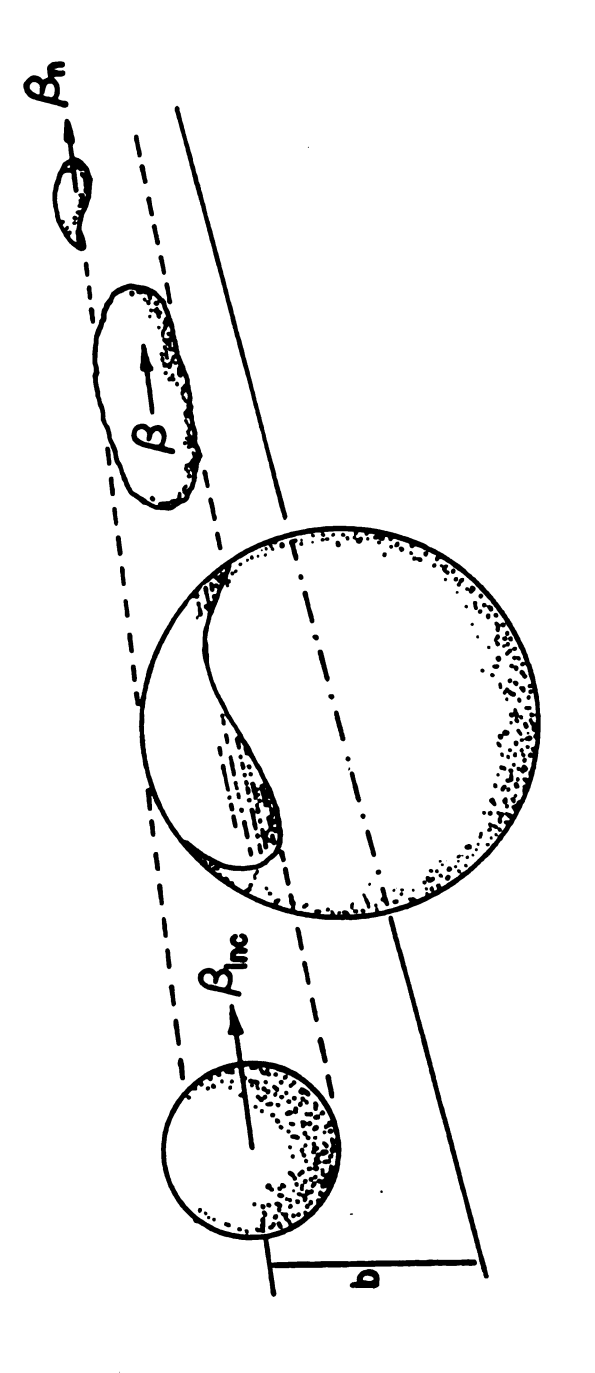
A simple way to estimate the number of nucleons in the source is the geometrical description given by the fireball $\operatorname{model}^{14,15}$. Figure 2.5 illustrates the geometry of the fireball model. The target and projectile are assumed to be spherical, with radii 1.2 x $\operatorname{A}^{1/3}$ fm, and they are assumed to make clean cylindrical cuts through each other. The fireball is composed of those nucleons in the target and in the projectile which are in the overlapping regions of the colliding nuclei. The remaining part of the target (and of the projectile, if the impact parameter is big enough) is the target spectator (and projectile spectator).

With these assumptions, it is possible to calculate the number of participant nucleons (i.e. the nucleons in the fireball) coming from the target, $N_{\rm t}$, and from the projectile, $N_{\rm p}$, as a function of impact parameter, b. The number of protons in the fireball is then given as the sum of the participating protons from the target plus the number of the participating protons from the projectile:

$$z_{tot}$$
 (b) = $\frac{z_t}{A_t} N_t$ (b) + $\frac{z_p}{A_p} N_p$ (b) (2.8)

where $Z_{t(p)}$ and $A_{t(p)}$ are the atomic and mass number of the target (projectile).

The model assumes that the projectile participants transfer all of their momentum to the fireball system, which moves along the beam direction at a velocity intermediate between those of the projectile and the target. Since the



nucleons from target and projectile are swept out to form a thermal source moving with velocity The overlapping a fireball. Formation of Figure 2.5.

internal kinetic energy per nucleon is much higher than the binding energy per nucleon, the fireball is treated as an equilibrated non rotating ideal gas of temperature T. It is assumed that the system expands isotropically in the center of mass of the fireball with a Maxwellian distribution in energy.

With these assumptions, the velocity of the fireball in the laboratory frame becomes:

$$\beta = \frac{P_{lab}}{E_{lab}} \tag{2.9}$$

where p_{lab} and E_{lab} are the momentum and total energy of the system in the laboratory frame. The total energy of the fireball in the center of mass is

$$E_{c.m.} = (E_{lab}^2 - p_{lab}^2)^{1/2}$$
 (2.10)

and the available kinetic energy per nucleon in the center of mass is:

$$\varepsilon = \frac{E_{c.m.}}{N_t + N_p} - m \qquad (2.11)$$

Assuming a relativistic ideal gas, the total energy in the center of mass is related to the temperature by the expression:

$$\frac{E_{C.m.}}{(N_p + N_t)T} = 3 + \frac{m}{T} \frac{K_1(m/T)}{K_2(m/T)}$$
 (2.12)

where K_1 and K_2 are MacDonald functions and m is the mass of a free nucleon. Non relativistically, the relation between and T is given for a classical gas simply by

$$\varepsilon = \frac{3}{2} T \tag{2.13}$$

The geometrical quantities (such as the number of protons in the fireball, Z_{tot} , the total number of nucleons in the fireball, N_{tot} , and the ratio N_{p}/N_{t} of projectile to target participant nucleons) and the kinematic quantities and can be calculated from the previous assumptions as a function of impact parameter. The momentum distribution of the fireball nucleons in the center of mass is given by

$$\frac{d^{2}N}{p^{2}dp \ d\Omega} = \frac{N}{4\pi m^{3}} \frac{e^{-E/T}}{2(T/m)^{2} K_{1}(m/T) + (T/m) K_{0}(m/T)}$$
(2.14)

or, non relativistically:

$$\frac{d^2N}{p^2dp\ d\Omega} = \frac{N}{(2\pi mT)^{3/2}} e^{-p^2/2mT}$$
 (2.15)

The spectra in the laboratory frame are obtained by transforming the above distribution to the laboratory, and finally summing over all impact parameters, weighting each impact parameter by $2\pi bZ_{tot}$.

In plotting the quantity $2\pi bZ_{tot}$ as a function of impact parameter ($b/(R_t+R_D)$), where R_t and R_D are the radii of the projectile and target nuclei), it is found that there is an impact parameter which has the maximum weight, (see Figures 2.6c, 2.7c, 2.8c). To find the number of nucleons in the fireball as a function as a function of impact parameter, one must calculate the volume of the intersection of a sphere and a cylinder. Numerical integration is necessary for an exact solution to this probapproximate analytical method has been developed. The results are summarized in Appendix B. largest inaccuracy obtained with the analytical formulae is about 6% when compared with the exact results from numerical integration.

The total number of nucleons in the fireball (N_{tot}) has been calculated as a function of b using the formulae in Appendix B, and from this the total number of protons Z_{tot} (equation 2.8) for the system analyzed here is deduced. The results are shown, as a function of $b/(R_p+R_t)$, in Figures 2.6a,b, 2.7a, b, and 2.8a,b. In Figures 2.6c, 2.7c, 2.8c the weight given to each impact parameter is plotted. Integrating the curves in a and b, weighting each point by $2\pi bZ_{tot}$, the "average" number of nucleons and protons in the fireball can be estimated. The results obtained from this integration have been used to estimate the "average" Coulomb energy experienced by a particle leaving the source:

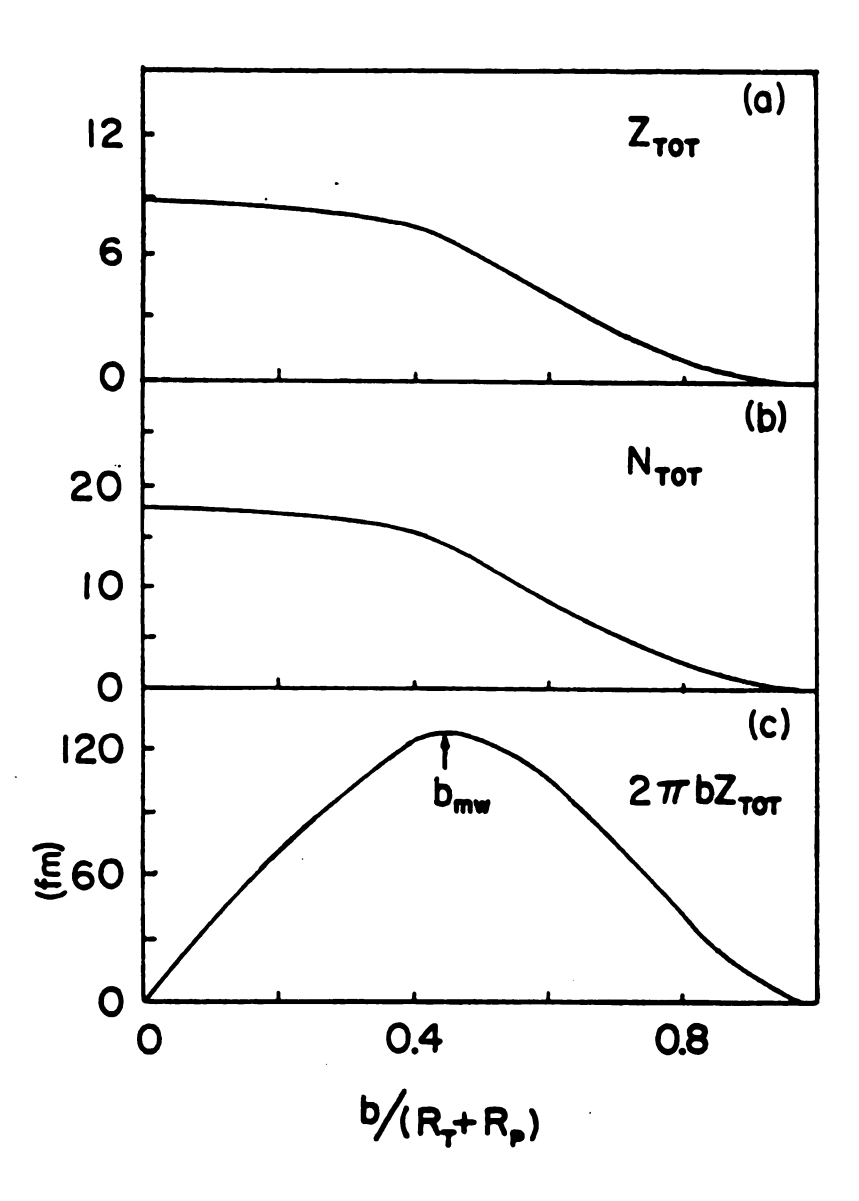


Figure 2.6. Geometrical quantities calculated for the system $\alpha+Ni$, as a function of impact parameter. (a) number of protons in the fireball, (b) total number of nucleons, (c) weight given to each impact parameter.

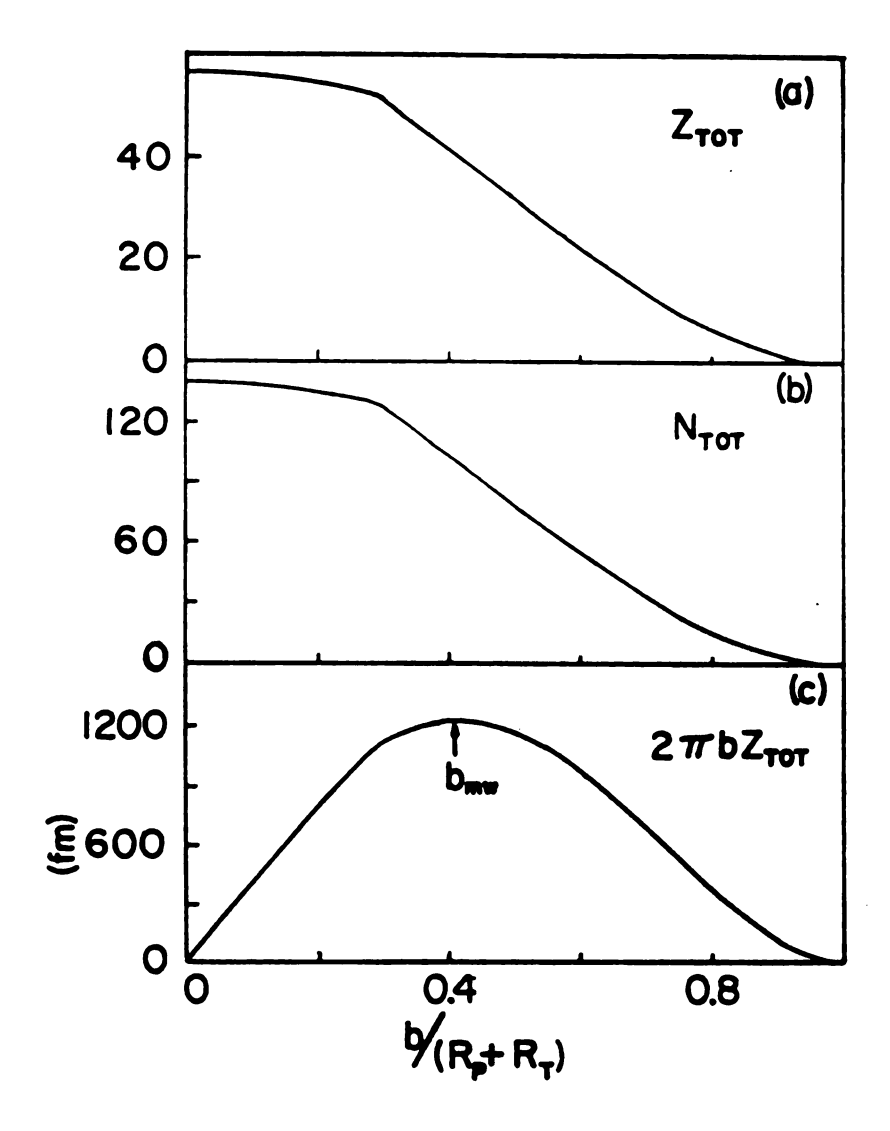


Figure 2.7. Geometrical quantities calculated for the system Ar+U, as a function of impact parameter.

(a) number of protons in the fireball,

(b) total number of nucleons, (c) weight given to each impact parameter.

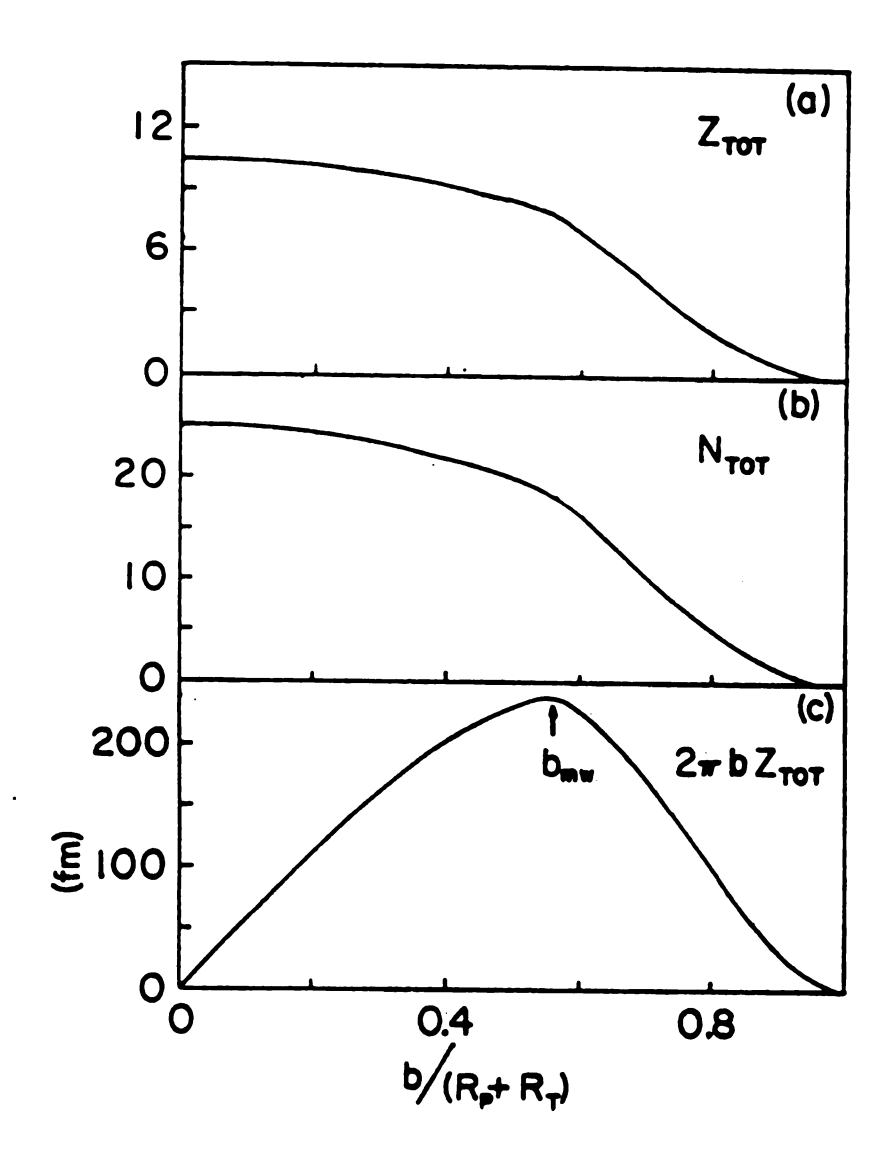


Figure 2.8. Geometrical quantities calculated for the system $\alpha+Ta$, as a function of impact parameter. (a) number of protons in the fireball, (b) total number of nucleons, (c) weight given to each impact parameter.

$$E_{c} = \frac{z_{source}^{xZ} frag}{1.4xN_{tot}^{1/3}}$$

where $\mathbf{Z}_{\mathtt{source}}$ is the average number of protons in the fireball minus the charge of the particle leaving the source $(\mathbf{Z}_{\mathtt{frag}})$ and $\mathbf{N}_{\mathtt{tot}}$ is the average number of nucleons in the source. The results obtained are summarized in Table 2.1. In the distribution used to fit the experimental data, the Coulomb energies derived in Table 2.1 have been devided by 2, to take into account the fact that during the emission of the fragments the charge of the source decreases, and the source is assumed to disintegrate completely for high temperatures ($200\,\mathrm{MeV}$).

Table 2.1. Average number of nucleons in the fireball ($N_{\rm tot}$), average number of protons ($Z_{\rm tot}$), and Coulomb energies for the systems analyzed.

System	N _{tot}	² tot	E _c (MeV)
α + Ta	18	8	2.8 (Z _{frag} =1) 4.7 (Z _{frag} =2)
a + Ni	12	6	2.2 (Z _{frag} =1)
Ar + U	88	36	35.8 (Z _{frag} =5)

Chapter 3

DATA ANALYSIS AND RESULTS

Inclusive spectra for various fragments, obtained at different energies and for different target-projectile systems have been fitted to the single moving source distribution derived in Chapter 2. For the reaction $\alpha+Ta$ at 180 MeV per nucleon , proton, deuteron, triton and 3 He spectra have been analyzed, together with proton spectra from the reaction $\alpha+Ni$ at beam energies of 100 and 173.5 MeV, and carbon and boron spectra from the Ar+U reaction at 100 MeV per nucleon.

Expression 2.7 has been used in a χ^2 -fit code (CHIFIT), to fit the experimental spectra and thus obtain the 'best' values of the three free parameters: temperature, velocity and total cross section, minimizing the χ^2 with respect to these parameters. The final values of T, v/c and $\sigma_{\rm e}$ obtained from the fitting procedure did not show a very strong dependence on the range of angles and energies included, even though the χ^2 values were very different. Typically, including in the fit the points obtained at angles smaller than 60 degrees gave a variation in the values of the parameters of about 1 to 5 %.

The influence of the value of the Coulomb repulsion energy ($\rm E_{\rm C}$) is even less significant, at least for light fragments, in which case the Coulomb interaction is not expected to be very strong ($\rm E_{\rm C} \leq 10 MeV$). The final

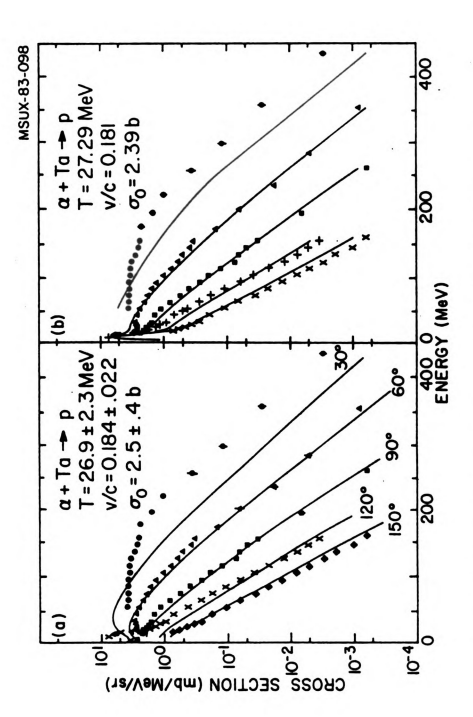
results for temperature and velocity do not appear to have a clear correlation with the value of $E_{\rm C}$, whereas the total cross sections decrease as $E_{\rm C}$ increases; this behaviour is expected, since one of the effects of such a change is to move the cut-off in the spectrum towards higher energies. In the case of light fragments, the variation of is not very large; for example, the decrease of the total cross section when $E_{\rm C}$ is varied from 1 to 10 MeV in the fitting of the proton spectra obtained in the α +Ta reaction is about 15% (from 2.445 to 2.036 b) , while T and v/c remain essentially the same in the two cases.

The choice of $E_{\rm C}$ appears to be more crucial for the analysis of heavy fragment spectra, because of its influence on the value of the total cross section. In the case of $^{12}{\rm C}$ emission, for instance, when $E_{\rm C}$ is varied from 55 to 25 MeV, the total cross section varies from .121 to .303 b, while temperature, velocity and the value of χ^2 remain essentially constant.

For consistency, and lacking a better criterion, the Coulomb energy has been calculated for all systems from the number of protons in the source, as obtained from the geometrical calculations of the fireball model, explained in Section 2.3. The errors on the best values of T, v/c, and σ , were estimated from the observations previously made on the changes of parameters and χ^2 -value, and from the experimental errors. The variations on the parameters are, therefore, chosen in such a way that the corresponding

increase in χ^2 is of about 20 to 25%. This was accomplished by using a computer program (ERFIT) which, for given values of one of the parameters, optimizes the others for minimum χ^2 .

Some of the experimental cross sections are shown and compared with the calculated curves in figures 3.1a, 3.2, 3.3, 3.4, 3.5. In these plots, experimental points at all and energies have been included, but it must be kept in mind that only the points at angles larger than or equal to 60 degrees and at energies larger than 30 MeV have been included in the fits. It is clear that the cross tions at more forward angles are greatly underestimated if only a single source is considered. Also, the peak which is observed at very low energies (see the spectra obtained for the reaction $\alpha+Ta$, figures 3.1, 3.2 and 3.3) is not accounted for in this simple parametrization. The hypothesis suggested in the previous chapter, that there could be a much slower source emitting low energy fragment and a faster source emitting preferentially in the forward direction, seems to be supported by the comparison of the experimental spectra with a three-source fit (figure 3.1b). In the case examined here, the proton spectra obtained from the c+Ta reaction, the low energy peak is well described including a slow ($\beta = .001$) source at low temperature (T=1.6 MeV) which may be identified with the target spectator in the fireball model. The inclusion of a third, fast source gives a higher cross section at forward angles, but does not



obtained for the intermediate energies. a) single moving Proton spectra for the a+Ta reaction, at an rapidity source are indicated. incident energy of 720 MeV. The final parameters source fit; source fit, 30 MeV were Figure 3.1.

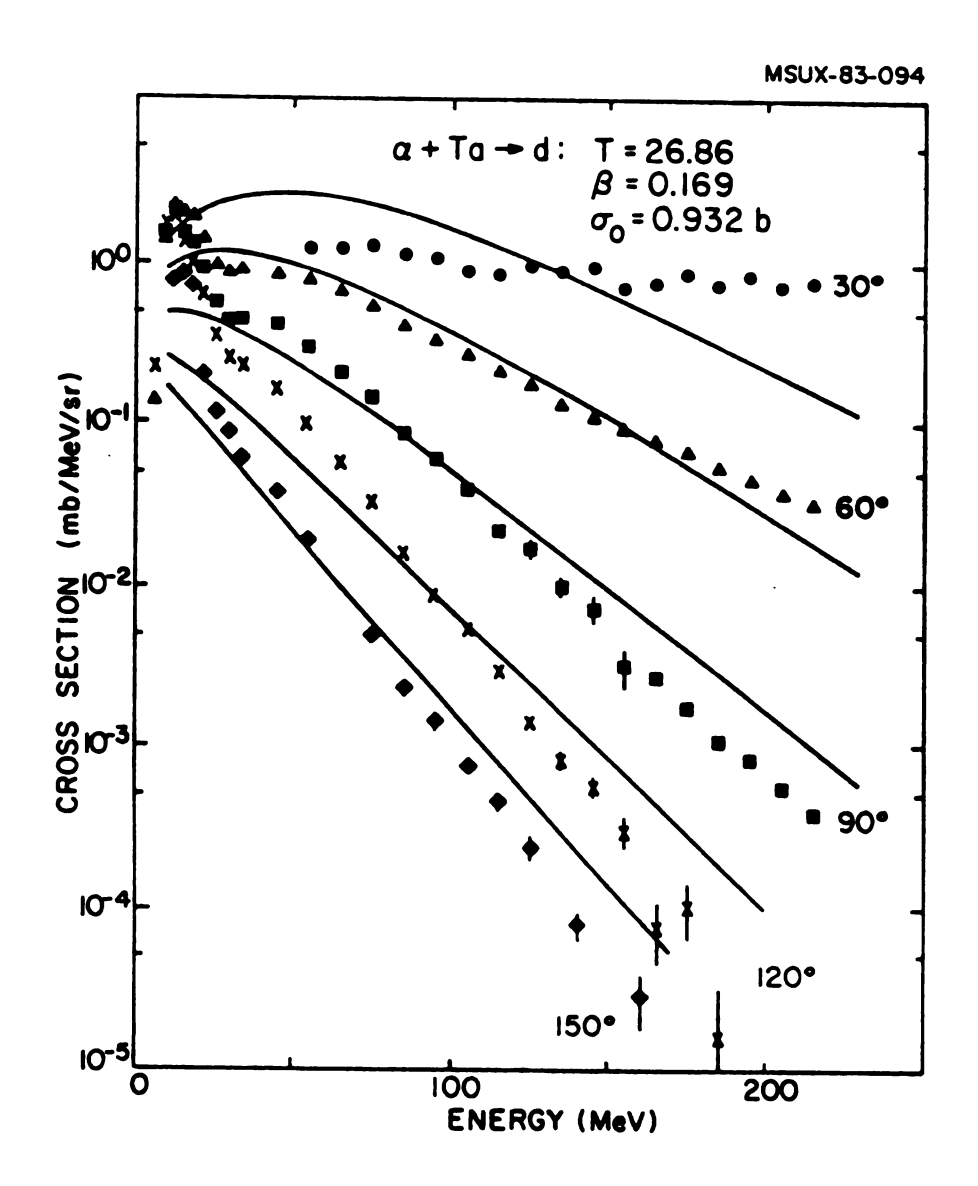


Figure 3.2. Deuteron spectra from the $\alpha+Ta$ reaction at 720 MeV. The final parameters, from which the solid curves are obtained, are T=26.86 MeV, v/c=0.169, σ_a =0.932 b.

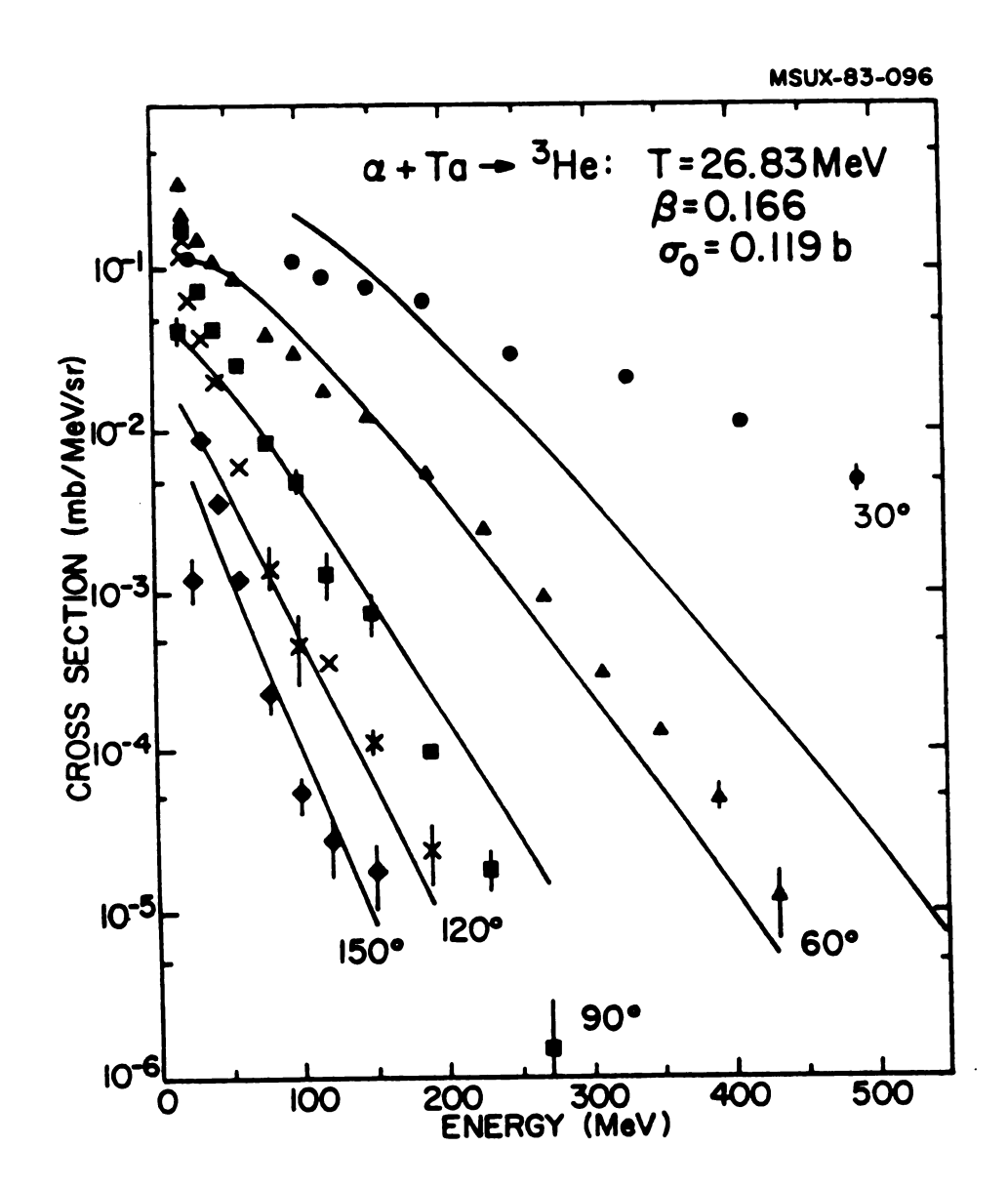


Figure 3.3. ³He spectra obtained from the reaction α +Ta at 720 MeV. The best fit gave: T=26.83 MeV, β =0.166, σ_{\bullet} =0.119 b.

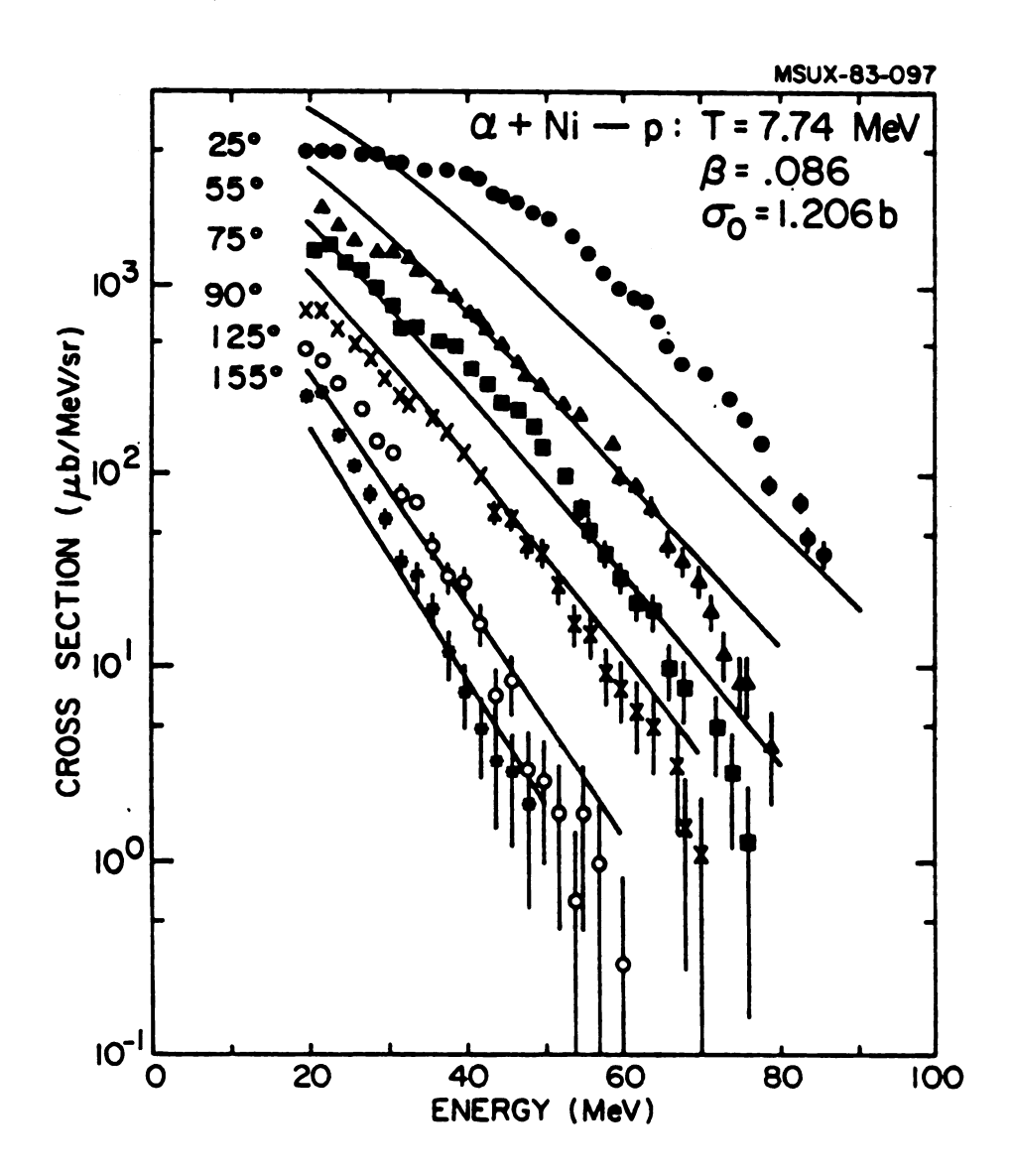


Figure 3.4. The experimental proton spectra obtained from the reaction $\alpha+Ni$ at 25 MeV per nucleon are plotted with the curves obtained from the χ^2 -fit with the following parameters: T=7.74 MeV, v/c=0.086, $\sigma_0=1.206$ b. The points at 25° were not included in the fit.

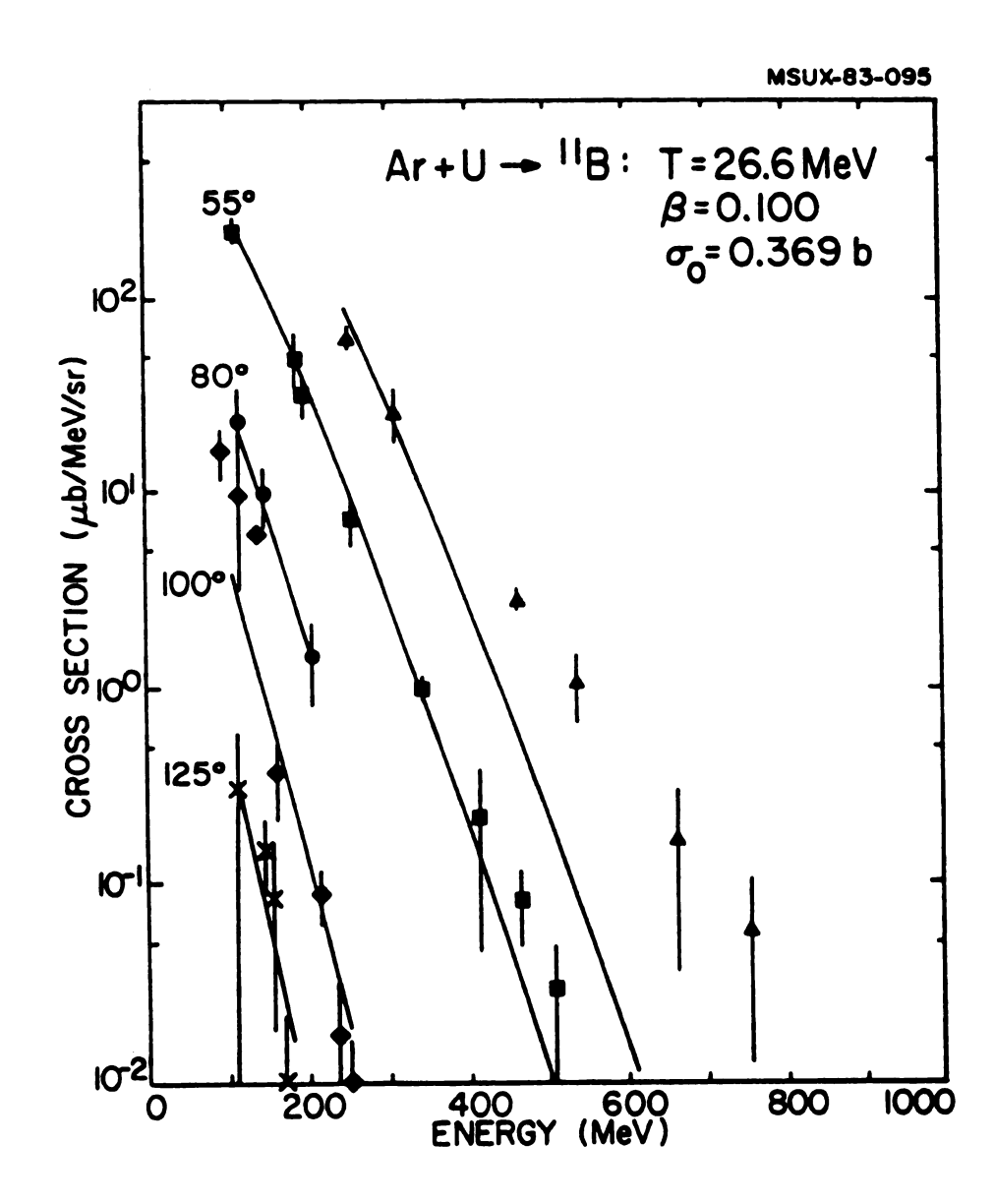


Figure 3.5. Experimental and calculated curves for the 11 B fragments obtained from the reaction Ar+U at 100 MeV per nucleon. The 'best fit' parameters are: T=26.6 MeV, v/c=0.100, $\sigma_{\rm e}$ =0.369 b. The points at 35° were not included in the fit.

change noticeably the curves at larger angles. Also, the fact that the 'intermediate' source parameters are essentially the same for the single- and the three-source fits, seems to support the idea that those parts of the spectra which have been analyzed here do indeed originate from a source with velocity intermediate between those of the target and the projectile, whose characteristics are well described by the simple single-source approximation.

The parameters obtained for the systems studied in . the present work are listed in table 3.1. In figures 3.6 and 3.7, the source temperatures and velocities are plotted for the systems discussed here (solid points) and, as a comparison, for the systems Ne+Au 19), O+Au 34) Ne+Pb³⁶) at various incident energies. Clearly, all the points follow the same general trend, suggesting that the hypothesis of a moving thermal source is equally valid for α -particle induced reactions as it is for heavier ions. Also, when different fragments are analyzed for a given colliding system, the temperatures and velocities obtained are the same, within the errors, for all fragments, indicating that they could all be emitted from a single This seems to be true also for fragments source. heavier than ⁴He, since the points for ¹¹B and ¹²C follow the general trend of the lighter fragments.

From the total cross sections, one can calculate the multiplicities for the emission of fragments. This has been done only in the case of protons, for which results at

Table 3.1. Summary of the relevant parameters for all the systems analyzed.

reaction	beam energy (MeV)	fragment	E _C (MeV)	a ((p)	T (MeV)	v/c source
α +Τα	720	Ω	1.4	2.4 ± 0.4	26.9 ± 2.3	Ø.184 ± Ø.022
a +Ta	720	ъ	1.4	Ø.93 ± Ø.23	26.86 ± 2.0	Ø.169 ± Ø.023
α +Ta	720	ų	1.4	0.29 ± 0.07	22.8 ± 1.8	Ø.12Ø ± Ø.015
a+Ta	720	3Не	2.4	0.12 ± 0.08	26.83 ± 2.9	Ø.166 ± Ø.036
a +Nİ	100	Q	1.1	1.21 ± 0.33	7.74 ± Ø.6	Ø.086±0.011
a +Ní	173.5	Q	1.1	Ø.99 ± Ø.15	10.96 ± .85	Ø.111 ± Ø.016
Ar+U	4000	11 B	18.0	Ø.37 ± Ø.20	26.6 ± 3.2	0.166 ± 6.014
Ar+U	4000	12 C	21.0	Ø.25 ± Ø.13	29.5 ± 3.9	0.082 ± 0.012

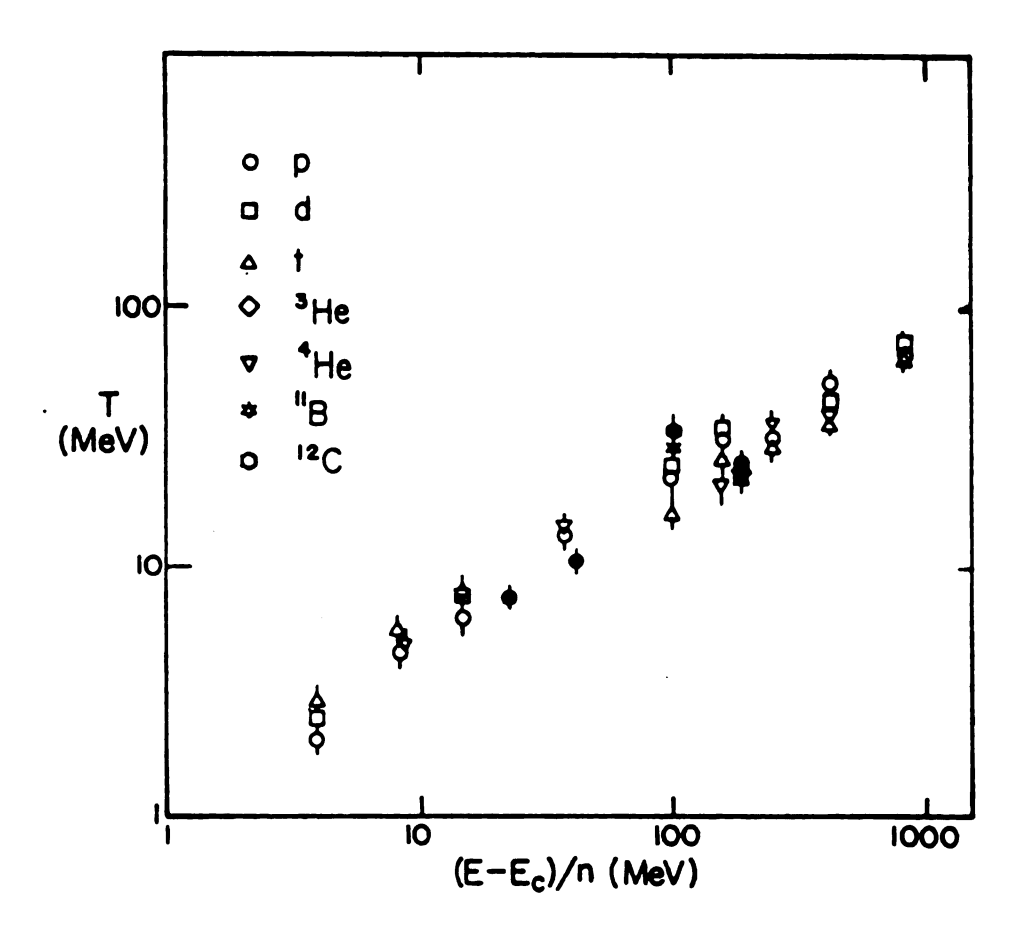


Figure 3.6. Source temperatures obtained from a χ^2 -fit. The solid points are for the systems analyzed in this work, the others are taken from reference 19.

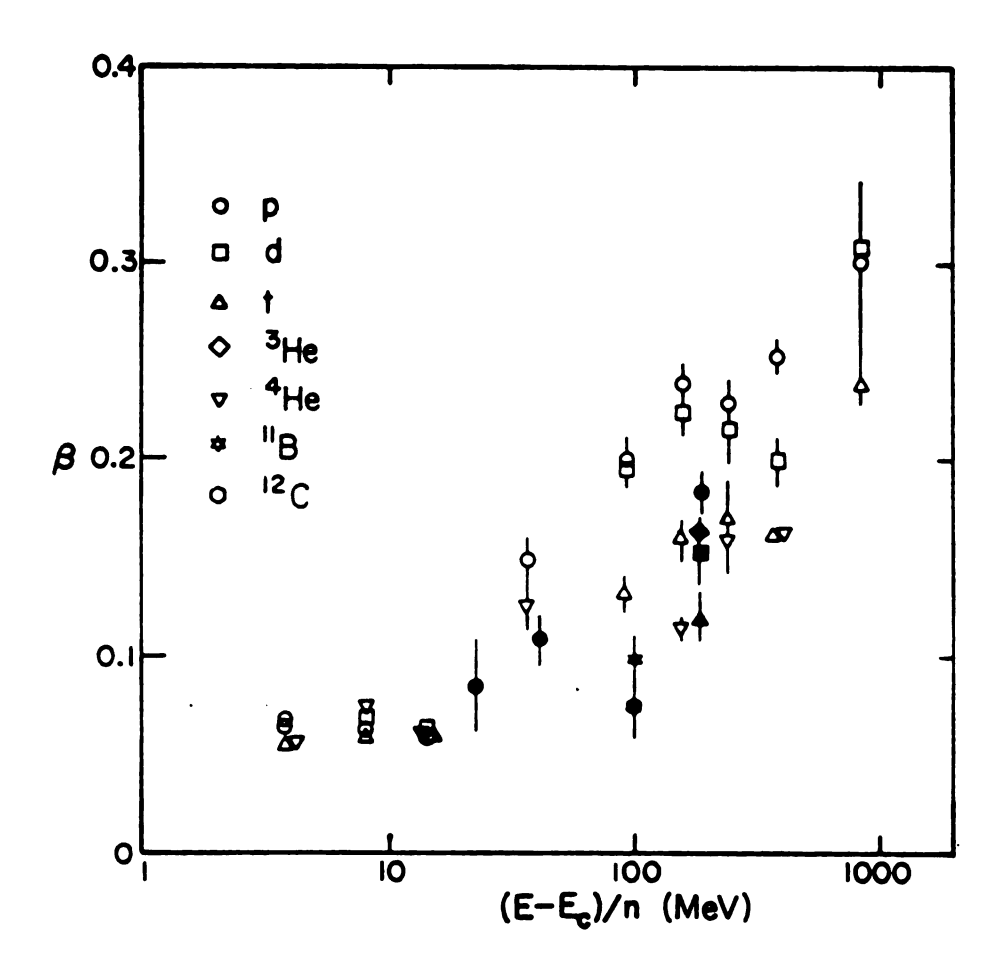


Figure 3.7. Source velocities obtained from a χ^2 -fit. The solid points are for the systems discussed in the present work; the others are taken from reference 19.

different energies are available. In order to compare multiplicities obtained for different systems, the results have been normalized following the geometrical assumptions of the fireball model. According to this prescription, the values obtained have been divided by the average total number of nucleons in the thermal source, as derived from fireball geometry. The normalized multiplicities, as a the function of the energy per nucleon, are plotted in figure 3.8 for protons emitted in α -particle induced reactions. The fact that only three points are available prevents us from drawing any final conclusions. All that can be said is that from 25 to 180 MeV per nucleon, the multiplicities change very little, indicating that the emisto sion process (number of protons emitted per unit size of the source) is the same in all cases. In view of a possible phase transition, it would be interesting to add more points at a temperature of about 20 MeV, to find if any sharp changes take place.

To conclude this analysis, a comparison was made with the case of α -fragments obtained from proton and deuteron induced reactions at energies of 90 and 40 MeV per nucleon, respectively $^{37,38)}$. A χ^2 -fit over the same range of angles and energies as discussed previously gave the following values for temperatures and velocities. For the proton induced reaction: T= 9.8 MeV and v/c= 0.04; for the deuteron induced reaction: T= 10.0 MeV and v/c= 0.03. These values of the parameters do not follow the trend found for

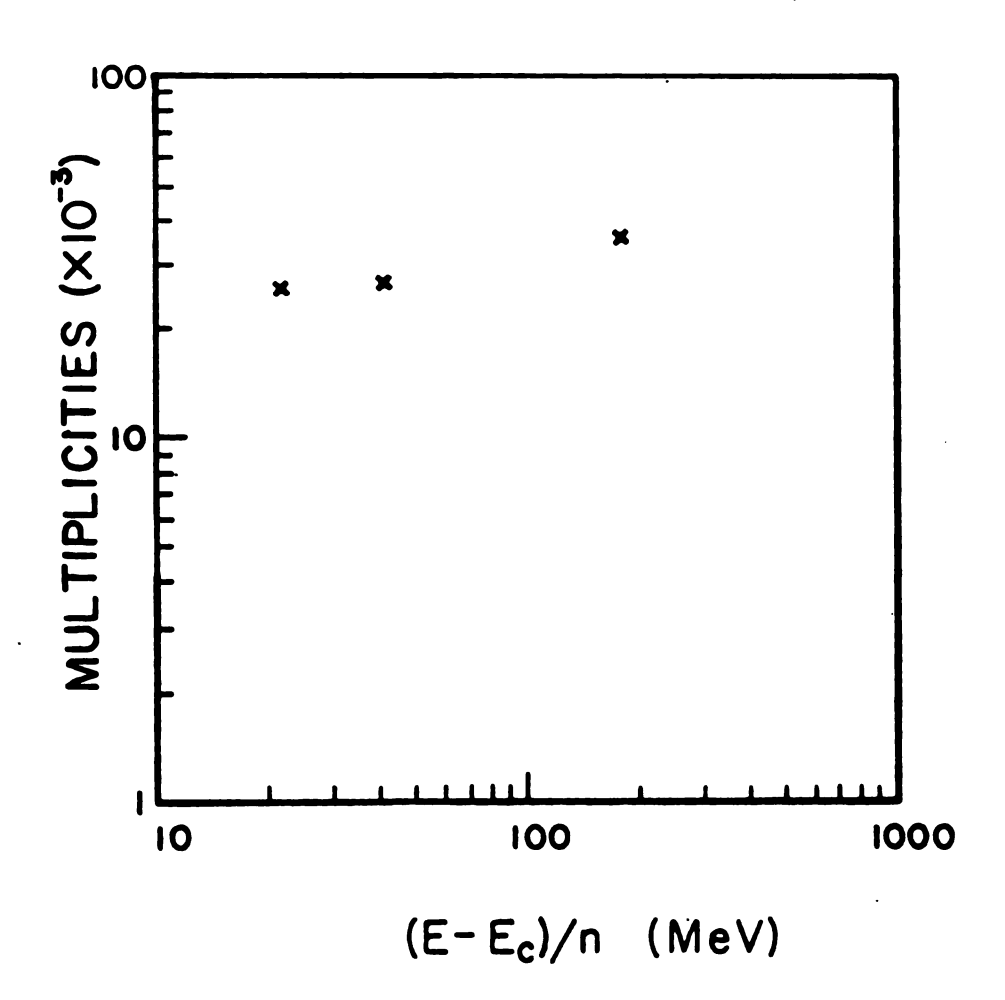


Figure 3.8. Normalized multiplicaties for emission of protons in a-particle induced reactions, as a function of the incident energy per nucleon.

a - and the heavy ion induced reactions, nor do the the calculated curves give a satisfactory agreement with the experimental points. In addition, unlike the curves discussed at the beginning of the chapter, the slopes of the energy spectra change very noticeably from angle to angle, showing that the hypothesis of an emitting source of well defined temperature is not justified in this case. For proton induced reactions, the high energy tails of the spectra of emitted particles are attributed to preequilibrium emission from states consisting of a few excitons (particle and hole excitation). Since the number of excitons changes significantly with each successive particle-hole creation, concept of a local temperature cannot be defined. In the case of heavy-ion induced reactions the initial exciton number is large and does not suffer such a large percentage change in the course of the emission. In this case more reasonable to define a local source temperature. The relation between this physical localization and the many exciton model remains to be explained.

Chapter 4

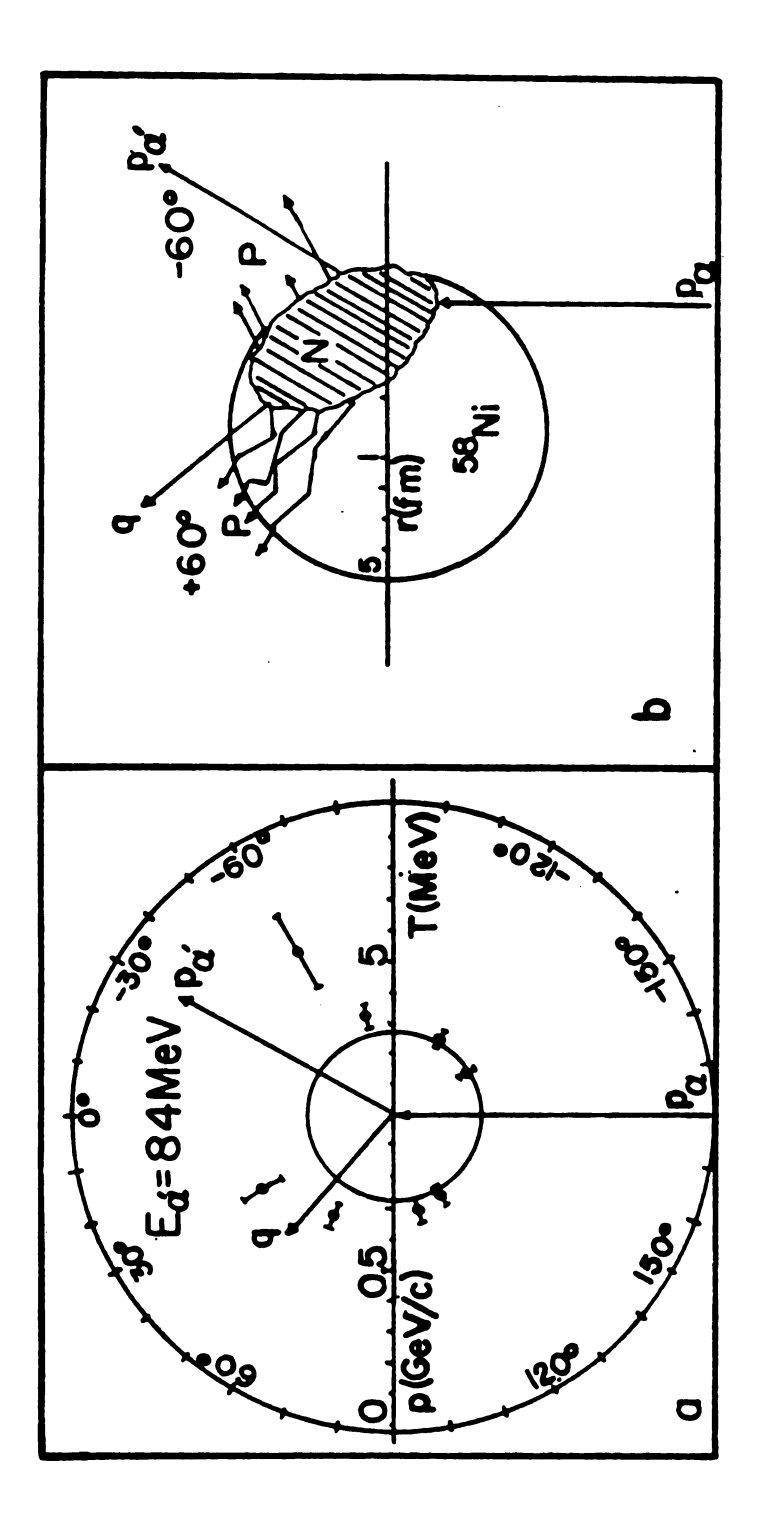
CONCLUSIONS

The first conclusion which can be drawn from the analysis presented in this work is about the presence of a thermal source. The systematic behaviour of parameters such temperature and velocity, which have been attributed as emitting source, demonstrates that the assumption to of the existence of such a source is well founded. Of particular importance is the fact that both heavy-ion and dparticle results follow the same trend, indicating that the basic assumptions of a thermal model (i.e. a rapid thermalization, involving a limited number of nucleons, and the fact that the characteristics of a localized source created in such a way do not depend on the size of the system, but only on the incident energy) are verified. A further confirmation, even though not conclusive, that the same kind of process is taking place over a large range of energies are the approximately constant values of the proton normalized multiplicities for incident energies from 25 to 180 MeV per nucleon.

Since proton spectra have also been explained as due to a knock-out process, it is especially meaningful that different fragments, from the same colliding system, appear to be originating from a source of given velocity and temperature. In particular, it must be noticed that heavy clusters such \$^{11}\$B\$ and \$^{11}\$C, which can hardly be expected to be produced in a knock-out type process, follow the same

systematics found for light fragments. The demonstration of the existence of a localized thermal source and the identification of a definite trend for the parameters which characterize such a source is important for the development of the thermal and hydrodynamical description of heavy-ion collisions.

In this work, no detailed assumptions were made about the characteristics of the thermal emitting source, and only for normalization purposes has a particular model (the fireball model) been adopted. In order to derive more information, experiments other than inclusive measurements are necessary. In recent coincidence experiments, a-projectiles have been used to measure the decay of a hot spot in ⁵⁸Ni(a , α' p) reaction at 35 MeV per nucleon 39 . When a temperature is ascribed to each proton spectrum (i.e. to each angle of emission), it is possible to derive an angular distribution for T. This angular distribution appears to be non symmetric about the direction of the transferred momentum q. In Figure 4.la the temperatures are shown as a function of the laboratory angle. Figure 4.1b shows a schematic picture of the mechanism which could cause such an asymmetry, namely a localized excited region in the target nucleus. In this picture, the asymmetry of the temperature angular distributions is due to the fact that protons emitted from the right hand side of the q-direction have gone a shorter way through nuclear matter than those emitted from the left hand side. These results contradict the model of a static



.(b) possible mechanism Figure 4.1. (a) angular dependence of the temperatures obtained for the Ni(G,G'p) reaction39 .(b) possible mechan causing the asymmetry observed in (a).

hot spot, since in the direction opposite to q temperatures close to those of the fully equilibrated systems are observed, but they do not permit a distinction between other different models like the quasi-free scattering model and the fireball or firestreak models, which give different explanations of the emission process.

The second type of information which one could derive from the kind of analysis presented in this work is about the possibility of phase transitions. It has been sugqested 31) that a liquid-gas phase instability could take place in the nuclear matter at temperatures below 20 MeV, which could influence the production of composite fragments. A high α/p ratio has indeed been observed at incident energies lower than 100 MeV/nucleon 19), but this could be a consequence of the large binding energy of a-particles. The study of heavier clusters is necessary to confirm the trend observed for α -fragments. In Figure 4.2 the weighted cross sections (i.e the cross sections multiplied by the mass number) for fragments of different mass are plotted as a function of the particle mass. The points for A ≥4 are taken from Ne+Au reaction 19) and suitably normalized to be compared with the points for ¹¹B and ¹²C. As a comparison, the values predicted by a the coalescence model have been calculated. In this model the cross section for fragment of mass A is related to that of a single nucleon (proton) by the following relation:

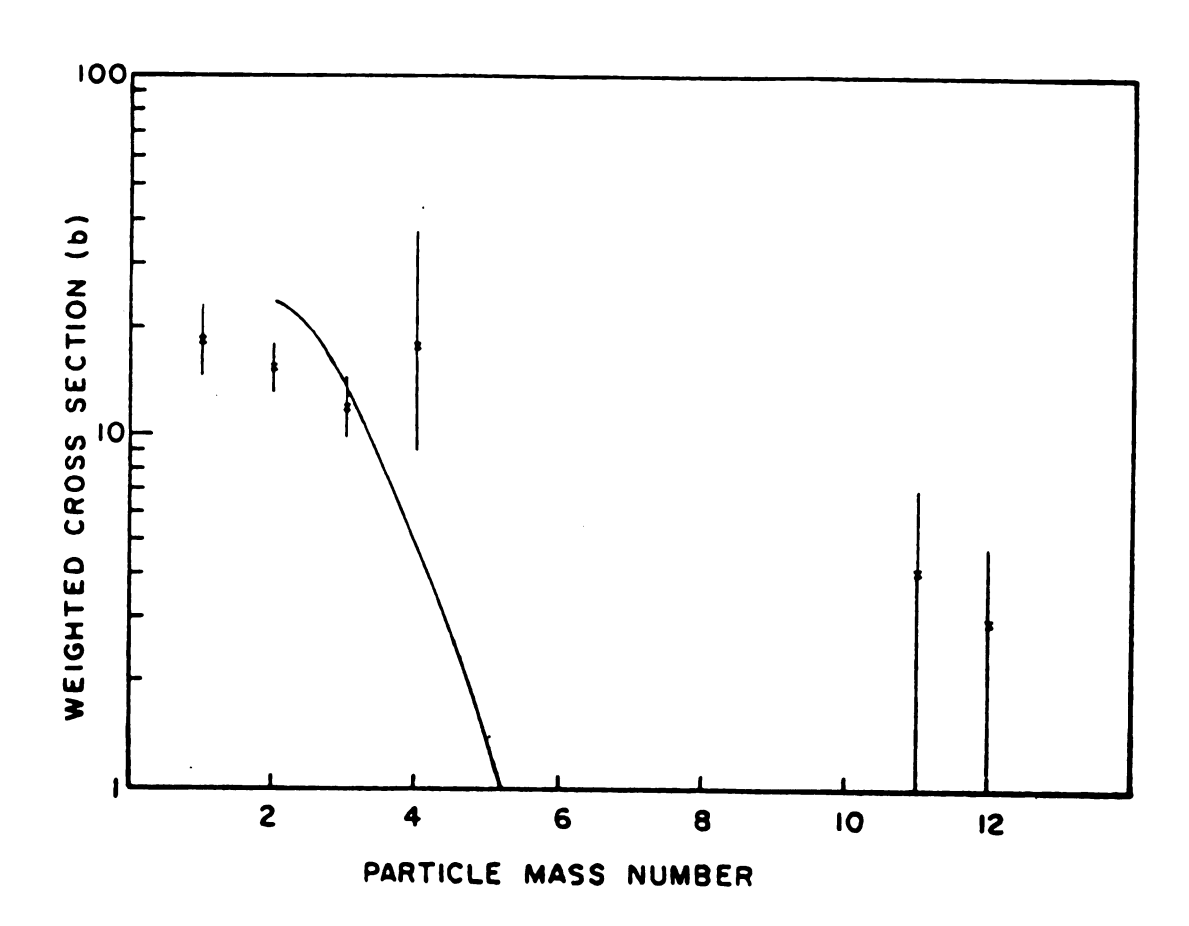


Figure 4.2. Weighted cross sections as a function of the fragment mass. The points for A \le 4 are taken from the reaction Ne+U at 100 MeV/nucleon, normalized for comparison with \$^{11}B\$ and \$^{12}C\$, obtained from Ar+U at the same incident energy. The curve represents the prediction of the coalescence model, with p =130 MeV/c.

$$\frac{d^2 \sigma_A}{p^2_A dp_A d\Omega} = \frac{1}{AI} \left(\frac{4\pi p^3_o}{3\sigma_o} \right)^{A-1} \left(\frac{d^2 \sigma_p}{p^2 dp d\Omega} \right)^{A}$$
(4.1)

where p_0 is the coalescence radius and σ_0 the reaction cross section. By integrating both sides of this equation, assuming a non relativistic Boltzmann distribution for $d^2\sigma/p^2dp\ d\Omega$ and setting y=1, it is possible to derive a relation between total weighted cross sections:

$$A\sigma_{A} = \frac{A^{3/2}}{(A-1)!} \left(\frac{4\pi p_{o}^{3}}{3\sigma_{o}}\right)^{A-1} (2\pi m_{T})^{3/2} \left(\frac{\sigma_{p}}{(2\pi m_{T})^{3/2}}\right)^{A} (4.2)$$

where A $\sigma_{\rm A}$ is the weighted cross section for fragments of mass A, as plotted in Figure 4.2 If the coalescence radius is assumed to be constant and equal to some typical values obtained from fitting experimental data ($p_{\rm O}$ =130 MeV/c was used here, taken from reference 15) the cross section for the heavy fragments is grossly underestimated, as can be seen in Figure 4.2, where the sharp fall-off predicted by the coalescence model is shown. The unexpected high yields experimentally observed for heavy clusters are indicative of a behaviour which cannot be explained in a simple gas model. At the present point there is not enough evidence to indicate that a phase transition is taking place, but these data clearly point out that further investigation in this direction is worth pursuing.

It has been suggested that a different kind of phase instability could be observed in heavy-ion collisions when a state of high density is created in nuclear matter due to a collision between heavy ions. The process can be followed in Figure 4.3. Here, The nuclear matter energy is plotted as a function of density for two values of entropy. During a collision which increases the density in addition increasing the internal energy, the system will move from a condition of equilibrium (e.g. point A) to a point of larger energy and higher density (say point B). If it can be assumed that little dissipation is associated with the subsequent expansion process, the system will then oscillate around the equilibrium state along the same isentrope, i.e. between points B and C. If the initial condition is in the overstressed zone, then the system has enough energy to reach the unstable region, where the compressibility of nuclear matter is negative. As mentioned before, the overstressed zone is more easily reached if the nuclear matter is compressed, since a lower amount of energy is necessary in this case. Therefore, a-particles do not seem to be as suited for the observation of this kind of instability as are heavier projectiles. A comparison of a -particle and heavy-ion induced reactions, both of which lead to the formation of a localized source, may therefore be a useful means of elucidating the influence of compression in nuclear collisions.

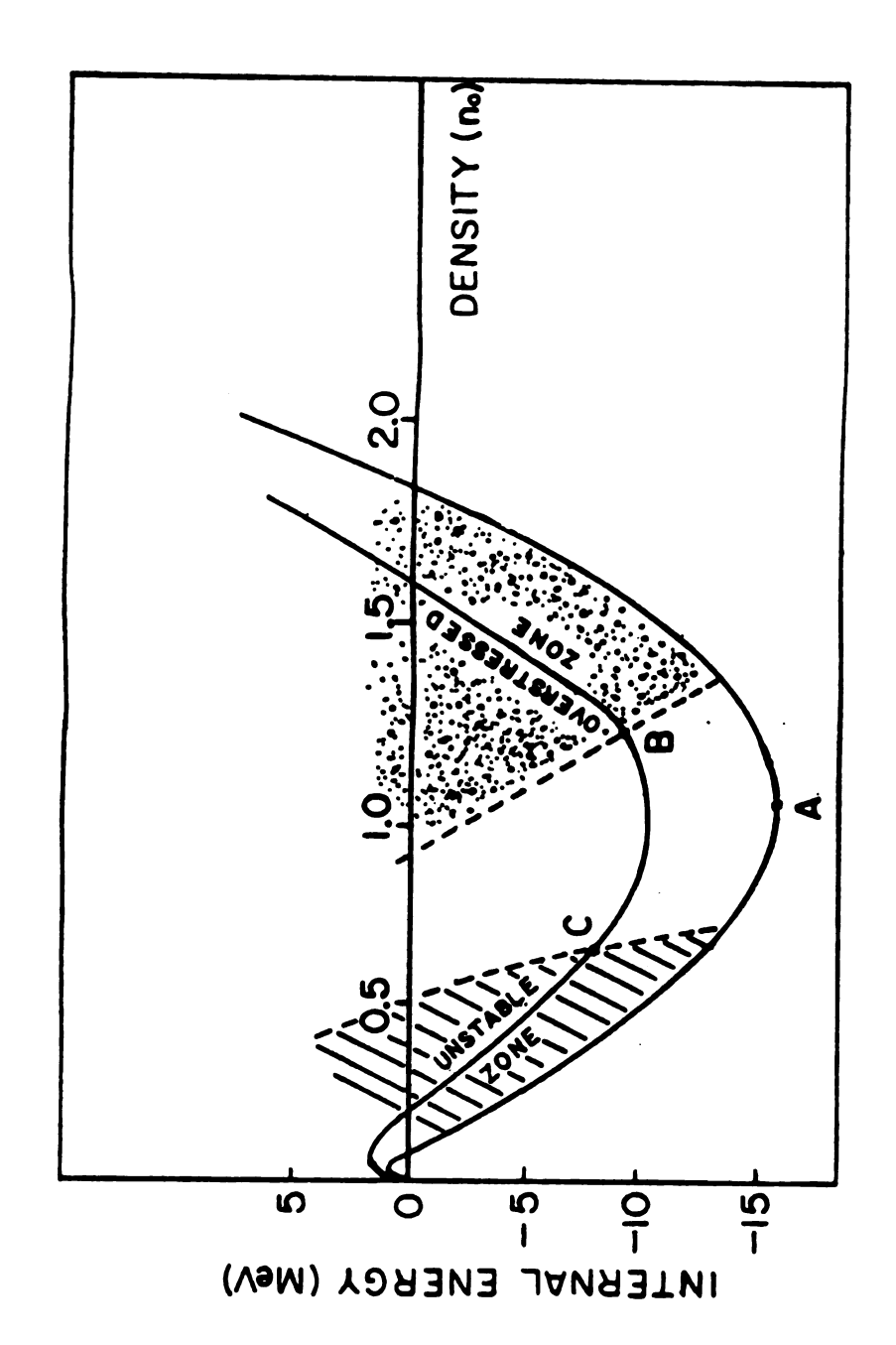
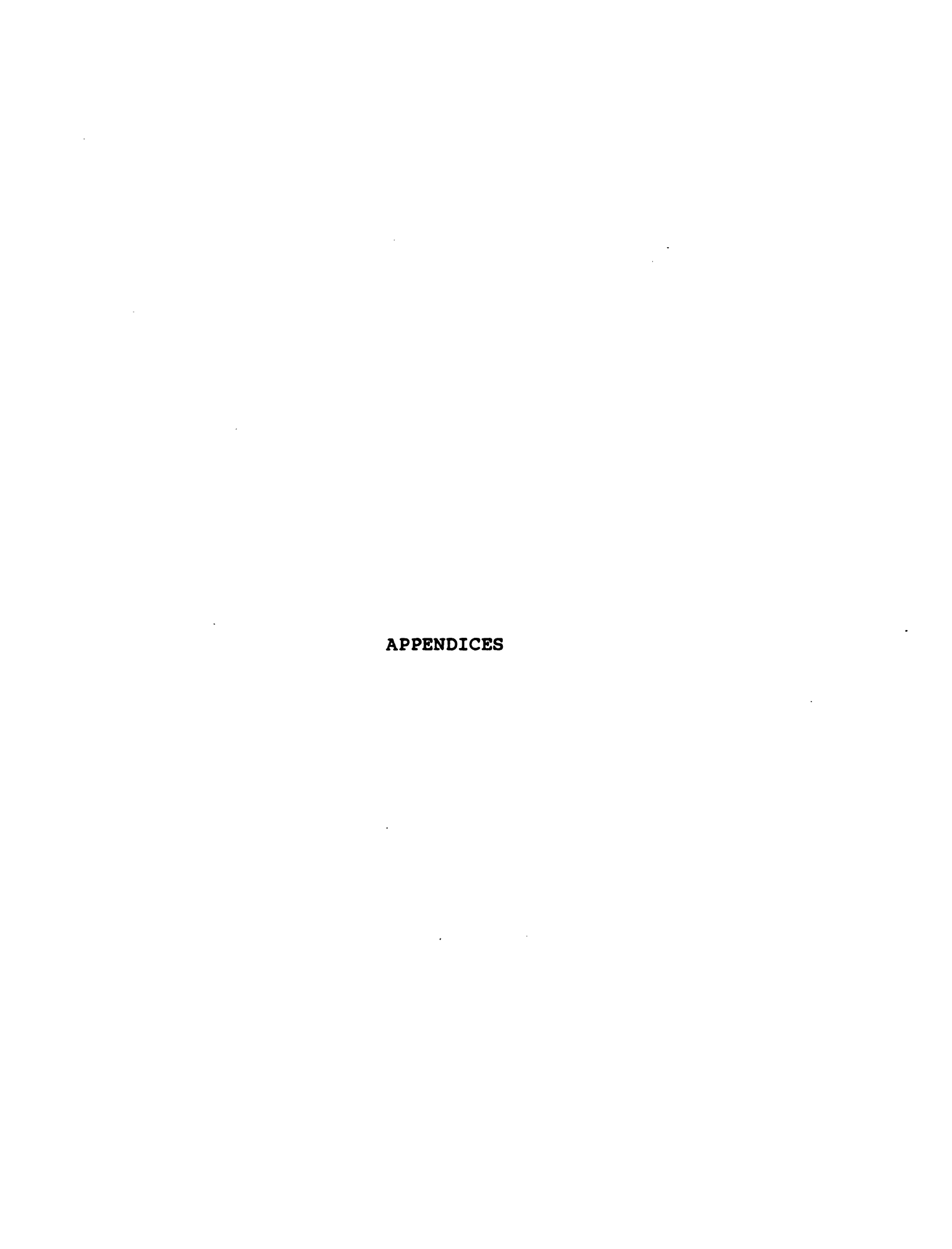


Figure 4.3. The energy-density plane for nuclear matter. The curves are isentropes.



APPENDIX A

RELATIVISTIC TRANSFORMATION OF DIFFERENTIAL CROSS SECTION 41)

In the following derivation, the unprimed coordinates refer to the laboratory system, the primed coordinates to the system of the moving source. The transformation is given by:

$$\frac{d^2\sigma}{dEd\Omega} = \frac{\delta(E'\Omega')}{\delta(E\Omega)} \frac{d^2\sigma'}{dE'd\Omega'}$$
 (A.1)

where the term $\frac{\delta(E'\Omega')}{\delta(E\Omega)}$ indicates the Jacobian of the transformation. This term can be rewritten as

$$\frac{\delta(E\Omega)}{\delta(E'\Omega')} = \frac{\delta(E\Omega)}{\delta(P\Omega)} \frac{\delta(P\Omega)}{\delta(P'\Omega')} \frac{\delta(P'\Omega')}{\delta(E'\Omega')} \tag{A.2}$$

indicating a sequence of three transformations: from energy to momentum variables in the source frame, from momentum in the source to momentum in the laboratory, and finally from momentum to energy in the new frame.

The Lorentz transformations for the 4-momentum will be used, assuming a common z-axis as the direction of motion:

$$P_{x} = P'_{x}$$

$$P_{y} = P'_{y}$$

$$P_{z} = y(P'_{z} + E')$$

$$E = y(E' + P'_{z})$$
(A.3)

First, the components of the 3-momentum will be written in terms of polar coordinates:

$$P_{x} = P \sin\theta \cos\phi$$

$$P_{y} = P \sin\theta \sin\phi \qquad (A.4)$$

$$P_{z} = P \cos\theta$$

The fact that $P_x = P'_x$ and $P_y = P'_y$ implies that $\phi = \phi'$, so the Lorentz transformations become:

$$P \cos\theta = y(P' \cos\theta' + E')$$

$$P \sin\theta = P' \sin\theta' \qquad (A.5)$$

$$E = y(E' + P' \cos\theta')$$

To find the second Jacobian in Equation A.2, we can transform in successive steps as follows:

$$\frac{\delta(P\Omega)}{\delta(P\Omega')} = \frac{\delta(P\Omega)}{\delta(P\Theta\phi)} \frac{\delta(P\Theta\phi)}{\delta(P\Phi\phi)}$$

$$\times \frac{9(b_1 x_b \lambda_b x)}{9(b_1 x_b \lambda_b x)} \frac{9(b_1 \theta_1 \phi_1)}{9(b_1 \phi_1 \phi_1)} \frac{9(b_1 \sigma_1)}{9(b_1 \sigma_1)}$$
(Y'9)

The first Jacobian is:

$$\frac{\partial(PQ)}{\partial(P\Theta\phi)} = \frac{dP \sin\Theta \ d\Theta \ d\phi}{dP \ d\Theta \ d\phi} = \sin\Theta \tag{A.7}$$

The second is just the Jacobian of the transformation between Cartesian and polar coordinates:

$$\frac{\delta(P\Theta\phi)}{\delta(P_x P_y P_z)} = \frac{1}{P^2 \sin\Theta}$$
 (A.8)

The last two Jacobians are the same as (A.7) and (A.8) for the primed coordinates.

For the factor in the middle, we have to refer to the Lorentz transformations and use the relation $E' = P'^2 + m^2$.

$$\frac{\delta(P_x P_y P_z)}{\delta(P_x P_y P_z)} = \frac{dP_x dP_y dP_z}{dP_x dP_y dP_z}$$
(A.9)

From Equation A.3 we obtain:

$$\frac{\partial(P_x P_y P_z)}{\partial(P_x P_y P_z)} = \frac{dP_z}{dP_z} = \frac{y(dP_z + dE_z)}{dP_z} = \frac{E}{E_z}$$
 (A.10)

Now, after multiplying all factors, we obtain:

$$\frac{\delta(P\Omega)}{\delta(P^{\dagger}\Omega^{\dagger})} = \frac{P^{\dagger}^{2}E}{P^{2}E^{\dagger}}$$
 (A.11)

For the first and third Jacobian in Equation A.2, we observe that

$$\frac{\delta(E\Omega)}{\delta(E'\Omega')} = \frac{\delta(E\Omega)}{\delta(P\Omega)} \frac{\delta(P\Omega)}{\delta(P'\Omega')} \frac{\delta(P'\Omega')}{\delta(E'\Omega')}$$
(A.12)

and

$$\frac{\delta(P\Omega)}{\delta(E'\Omega')} = \frac{\delta(P\Omega)}{\delta(P'\Omega')} \frac{\delta(P'\Omega')}{\delta(E'\Omega')} = \frac{P'E}{P^2}$$
 (A.13)

And, finally, we can derive the expression for the Jacobian in Equation A.2:

$$\frac{\delta(E\Omega)}{\delta(E'\Omega')} = \frac{P'}{P} \tag{A.14}$$

Thus we obtain

$$\frac{d^2\sigma}{dEd\Omega} = \frac{P}{P'} \frac{d^2\sigma'}{dE'd\Omega'}$$
 (A.15)

APPENDIX B

ANALYTICAL EXPRESSIONS FOR THE FIREBALL GEOMETRY

The number of participant nucleons in a spherical nucleus of mass number A_1 and radius R_1 which collides with impact parameter b with a spherical nucleus of mass A_2 and radius R_2 is given by 15 :

$$N_1 = A_1 F((/, \delta))$$
 (B.1)

where the parameters / and 6 are defined as

$$(/ = \frac{R_1}{R_1 + R_2}$$
 (B.2)

$$\delta = \frac{b}{R_1 + R_2} \tag{B.3}$$

and the analytical expression of the function F depends on the sector in the δ , $\langle \rangle$ plane as represented in Figure B.1. The expressions for F in the four sectors are the following:

$$F_I = (1-(1-\mu^2)^{3/2}) (1-(\frac{\delta}{V})^2)^{1/2}$$

$$F_{II} = \frac{3}{4} (1-t)^{1/2} (\frac{1-\delta}{t})$$

$$-\frac{1}{8} \left[\frac{3(1-\sqrt{t})^{1/2}}{\mu} - \frac{(1-(1-\mu^2)^{3/2})(1-(1-\mu)^2)^{1/2}}{\mu^3} (\frac{1-\delta}{\sqrt{t}})^3 \right]$$

$$F_{\text{III}} = \frac{3}{4} (1 - (/)^{1/2} (\frac{1 - \delta}{\sqrt{2}})^2 - \frac{1}{8} (3(1 - (/)^{1/2} - 1) (\frac{1 - \delta}{\sqrt{2}})^3$$

$$F_{TV} = 1$$

where $\mu = \frac{R_2}{R_1}$. The four sectors correspond to the following situations:

- I. A cylindrical hole is gouged in the nucleus 1, which is larger than 2.
- II. A cylindrical channel is gouged in 1, with a radius smaller than $\boldsymbol{R}_{\boldsymbol{1}}$.
- III. A cylindrical channel is gouged in 1, with a radius larger than $\boldsymbol{R}_{\boldsymbol{l}}$.
- IV. All of nucleus 1 is obliterated by nucleus 2, and R_2 > R_1 .

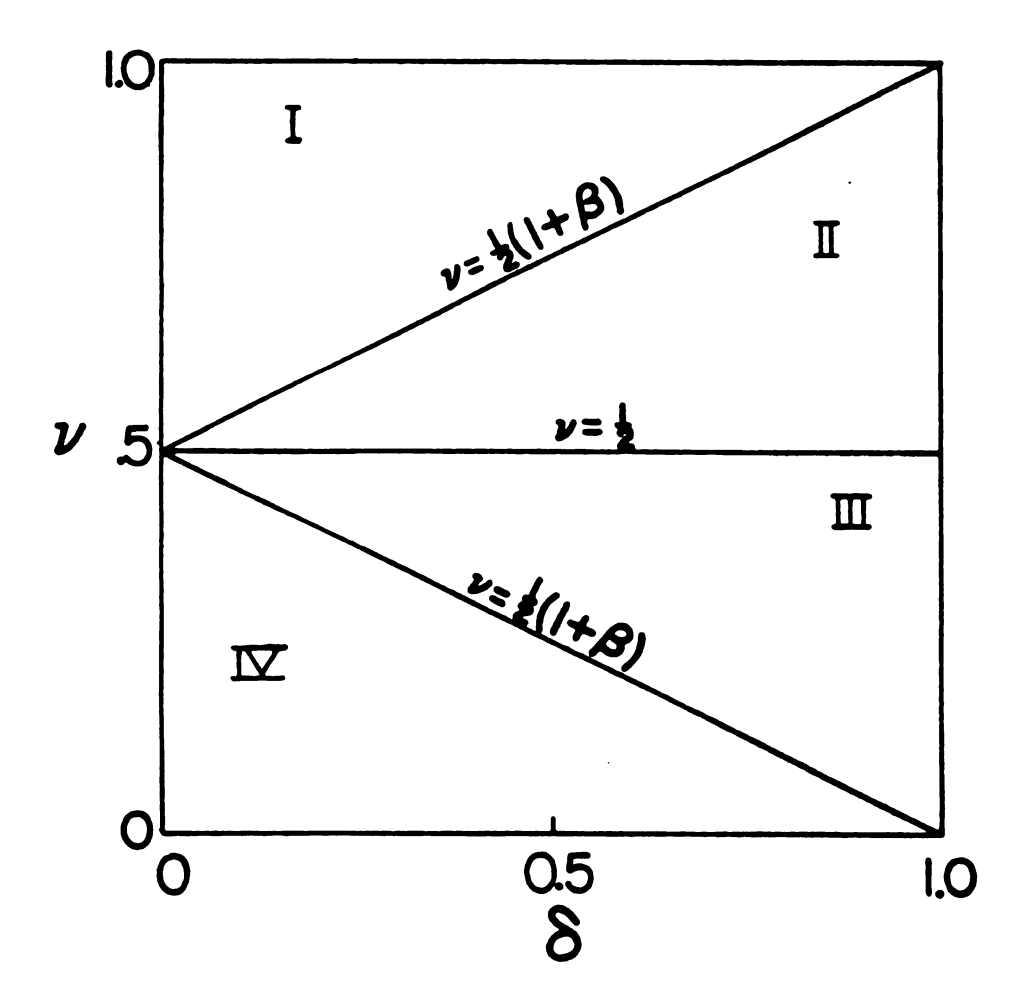


Figure B.1. Definition, in the (δ, ν) plane, of the regions where the four F functions must be applied.

LIST OF REFERENCES

LIST OF REFERENCES

- [1] Y.Eyal, A.Gavron, I.Tserruya, Z.Fraenkel, Y.Eisen, S.Wald, R.Bass, G.R.Gould, G.Kreyling, R.Renfordt, K.Stelzer, R.Zitzmann, A.Gobbi, U.Lynen, H.Stelzer, I.Rode and R. Bock, Phys.Rev.Lett. 41, 625 (1978)
- [2] D.Hilscher, J.R.Birkelund, A.D.Hoover, W.U.Schroder, W.W.Wilcke, J.R.Huizenga, A.C.Mignerey, K.L.Wolf, H.F.Breuer and V.E.Viola, Jr., Phys.Rev. C20, 576 (1979)
- [3] M.Blann, Nucl. Phys. A235, 211 (1974)
- [4] T.J.M.Symons, P.Doll, M.Bini, D.L.Hendrie, J.Mahoney, G.Mantzouranis, D.K.Scott, K.van Bibber, Y.P.Viyogy, H.H.Wieman and C.K.Gelbke, Phys. Lett. 94B, 131 (1980)
- [5] H.W.Bertini, R.T.Santoro and O.W.Hermann, Phys. Rev. C14, 590 (1976)
- [6] J.Cugnon, Phys. Rev. C22, 1885 (1980)
- [7] J.P. Bondorf, J.N. De, A.O.T. Karvinen, G. Fai and B. Jakobsson, Phys. Lett. 84B, 162 (1979)
- [8] J.P. Bondorf, J.N. De, A.O.T. Karvinen, G. Fai, B. Jakobsson and J. Randrup, Nucl. Phys. A333, 285 (1980)
- [9] P.A. Gottschalk and M. Westrom, Phys. Rev. Lett. 39, 1250 (1977)
- [10] P.A. Gottschalk and M. Westrom, Nucl. Phys. A314, 232 (1979)
- [11] S.I.A. Garpman, D. Sperber and M. Zielinska-Pfabe, Phys. Lett. 90B, 53 (1980)
- [12] S.I.A. Garpman, S.K. Samaddar, D. Sperber and M. Zielinska-Pfabe, Phys. Lett. 92B, 56 (1980)
- [13] N. Stelte and R. Weiner, Preprint 1982

- [14] G.D. Westfall, J. Gosset, P.J. Johansen, A.M. Poskanzer, W.G. Meyer, H.H. Gutbrod, A. Sandoval and R. Stock, Phys. Rev. Lett. 37, 1202 (1976)
- [15] J. Gosset, H.H. Gutbrod, W.G. Meyer, A.M. Poskanzer, A. Sandoval, R. Stock and G.D. Westfall, Phys. Rev. C16, 629 (1977)
- [16] J. Gosset, J.I. Kapusta and G.D. Westfall, Phys. Rev. C18, 844 (1978)
- [17] W.G. Meyer, Nucl. Phys. A269, 177 (1978)
- [18] T.C. Awes, G.Poggi, C.K. Gelbke, B.B. Back, B.G. Glagola, H. Breuer and V.E. Viola, Jr., Phys. Rev. C24, 89 (1981)
- [19] G.D. Westfall, B.V. Jacak, N. Anantaraman, M.W. Curtin, G.M. Crawley, C.K. Gelbke. B. Hasselquist, W.G. Lynch, D.K. Scott, B.M. Tsang, M.J. Murphy, T.J.M. Symons, R. Legrain, and T.J. Majors, Phys. Lett. 116B, 118 (1982)
- [20] K.R. Cordell, S.T. Thornton, L.C. Dennis, R.R. Doering, R.L. Parks and T.C. Schweitzer, Nucl. Phys. A362, 431 (1981)
- [21] R. Santo, Private Communication
- [22] K.A. Frankel and J.D. Stevenson, Phys. Rev. C23, 1511 (1981)
- [23] R. Weiner and M. Westrom, Phys. Rev. Lett. 34, 1523 (1975)
- [24] R. Weiner and M. Westrom, Nucl. Phys. A286, 282 (1977)
- [25] S. Tomonaga, Z. Phys. 110, 571 (1936)
- [26] A.K. Dhar and B.S. Nilsson, Nucl. Phys. A315, 445 (1979)
- [27] H.H. Gutbrod, A. Sandoval, P.J. Johansen, A.M. Poskanzer J. Gosset, W. G. Meyer, G.D. Westfall, and R. Stock, Phys. Rev. Lett. 37, 667 (1976)
- [28] M.C. Lemaire, S. Nagamiya, S. Schnetzer, H. Steiner and I. Tanihata, Phys. Lett. 85B, 38 (1979)
- [29] A. Mekjian, Phys. Rev. Cl7, 1051 (1978)
- [30] A. Mekjian, Phys. Lett. 89B, 177 (1980)

- [31] M. Curtin, H. Toki and D.K. Scott, M.S.U. Preprint
- [32] A.S. Goldhaber, Phys. Rev. C17, 2243 (1978)
- [33] O. Scholten, Private Communication
- [34] T.C. Awes, G. Poggi, S. Saini, C.K. Gelbke, R. Legrain and G.D. Westfall, Phys. Lett. 103B, 417 (1981)
- [35] J.B. Natowitz, M.N. Namboodiri, L. Adler, R.P. Schmitt, R.L. Watson, S. Simon, M. Berlanger and R. Choudhury, Phys. Rev. Lett. 47, 1114 (1981)
- [36] S. Nagamiya, M.C. Lemaire, E. Moeller, S. Schnetzer, G. Shapiro, H. Steiner and I. Tahinata, Phys. Rev. C24, 971 (1981)
- [37] J.R. Wu, C.C. Chang and H.D. Holmgren, Phys. Rev. C19, 370 (1979)
- [38] J.R. Wu, C.C. Chang and H.D. Holmgren, Phys. Rev. C19, 698 (1979)
- [39] U. Bechstedt, H. Machner, A. Budzanowski, P. Jahn and C. Meyer-Boricke, Preprint
- [40] G.F. Bertsch, to be published in ICNNC Proceedings
- [41] R. Hagedorn, Relativistic Kinematics, W.A. Benjamin (1963)

